TECHNICAL REPORT NO. WAL TR 310.24/5-4

METALLURGICAL ASPECTS OF FRACTURE AT HIGH STRENGTH LEVEL

Final Technical Report

Prepared by

Walter A. Backofen

and

Merrill L. Ebner
Massachusetts Institute of Technology

May 1963

Contract No. DA-19-020-ORD-5235
Boston Procurement District, U.S. Army
Ordnance Management Structural Code 5010.11.843
Department of the Army Project No. 5B93-32-004

Watertown Arsenal Laboratories
Watertown, Massachusetts

The findings in this report are not to be construed as an official Department of the Army position.

ASTIA AVAILABILITY NOTICE

Qualified requesters may obtain copies of this report from ASTIA.

DISPOSITION INSTRUCTIONS

Destroy; do not return.

FILING SUBJECTS:

1. Steel, Physical and Mechanical Properties
2. Fracture Toughness
3. Rocket Motor Cases

METALLURGICAL ASPECTS OF FRACTURE AT HIGH STRENGTH LEVELS

Final Technical Report

Prepared by

Walter A. Backofen

and

Merrill L. Ebner
Massachusetts Institute of Technology

May 1963

Contract No. DA-19-020-ORD-5235
Boston Procurement District, U.S. Army
Ordnance Management Structural Code 5010.11.843
Department of the Army Project No. 5B93-32-004

Watertown Arsenal Laboratories
Watertown, Massachusetts

ABSTRACT

PLANE-STRAIN FRACTURE IN AISI 4340 STEEL

The plane-strain fracture toughness of quenched and tempered AISI 4340 steel was measured in tension at room temperature with circumferentially notched and fatigue-cracked specimens. Values of G_{IC} for indicating the variation encountered were 5.6, 23, and 254 in-lbs/in^2 after tempering at 212, 400, and 800°F, respectively.

Cracking characteristics were influenced by tempering temperature. Below about 700°F, little stable crack growth was found and propagation occurred in a mixed mode that appeared to consist at least partly of cleavage fracture. At higher temperatures, initial cracking was stable and developed by a ductile shear process; rapid fracturing again occurred in a mixed mode. After tempering at 1000°F and above, fracture was ductile.

I. INTRODUCTION

A. A. Griffith(1) suggested in 1920 that a crack in a brittle material will propagate when the energy absorbed by the advancing crack on incremental extension equals the change in the energy of the elastic stress-field. For the case of a short crack of length 2c in an extensive sheet under plane-stress, Griffith obtained(2)

$$\sigma = \sqrt{\frac{qE}{\pi c}} \tag{1}$$

where

σ = average stress normal to the crack (gross stress) at which the crack will propagate

E = Young's Modulus

q = energy absorbed as the crack of length 2c extends to cover a new unit of area

In the early experiments, breaking stress measurements were in good agreement with values of σ calculated from Eq. (1) when q was taken as twice the estimated surface energy, γ. In Shand's(3,4) extensive work on the fracture of glass, however, only specimens broken in air at low loading rates (by static fatigue) failed at stresses corresponding to $q = 2\gamma$; higher rates of loading were associated with values of q as much as 50 times greater than 2γ.

Irwin(5) and Orowan(6) both realized that the Griffith approach could be applied to metals in which significant amounts of work are absorbed through plastic deformation as the crack advances. The problem was to obtain the proper expression for q in Griffith's equation. Writing $q = G_c$ to be consistent with contemporary notation, their two equivalent suggestions were:

$$\left.\frac{d W_E}{d A}\right|_c = G_c = p + 2\gamma \tag{2}$$

where W_E is the elastic energy in the system, A is the surface area of the largest crack present, c indicates instability, and p is the energy absorbed by plastic deformation of material adjacent to the crack as it extends over unit area.

The approach adopted by Irwin was to compute $(dW_E/dA)_c$, while that of Orowan was to estimate p. Irwin observed that for many conditions of stress and geometry, the elastic strain energy, W_E, in a specimen containing a sharp crack could be calculated from the elastic stress field; on this basis a relationship was obtained between $(dW_E/dA)_c$ (or G_c) and the stress field for a specimen tested in a rigid machine.(7) Bueckner(8) later showed that the same value of G_c is obtained in either a rigid or soft (dead-load) machine. The success of Irwin's treatment rests on the relatively small error resulting from the unknown stress state in the plastic zone at the crack tip. Analyses have since been published for a variety of loading configurations(9,10,11,12).

Orowan, on the otherhand, noted that $p \gg 2\gamma$ and then sought to evaluate p, which is a problem of extraordinary experimental difficulty. Orowan and Felbeck(13) attempted to estimate p from X-ray measurements on the brittle fracture surfaces of mild steel. Their success was limited because of the qualitative nature of the measurements and the large variations in p derived from crack acceleration and deceleration in a strain-rate sensitive material such as mild steel.

At present the parameter G_c, or plane-stress fracture toughness, is widely used to describe the notch toughness of sheet materials. The parameter K_c, also a measure of fracture toughness, is related to G_c by the expression $K_c^2 = G_c E$, where E is Young's modulus. G_c has the advantage of being easily visualized as an analog to the surface energy, whereas K_c has the advantage of being directly proportional to the stress at fracture. The fracture surface of a broken sheet specimen for determining G_c or K_c typically consists of shear lips along the edges and flat fracture in the interior, the relative proportions depending upon the sheet thickness and testing temperature. The parameters G_{IC} and K_{IC} are indices of fracture toughness analogous to G_c and K_c but relating now to conditions of plane strain. The circumferentially notched tensile specimen seems to represent the best approach to measurement of G_{IC}. In this specimen, all fracture is of the flat type; that is, no shear lips are formed. Measurements in the present work were made with such specimens.

II. EXPERIMENTAL PLANE-STRAIN FRACTURE DATA FOR AISI 4340 STEEL

Air-melted aircraft quality AISI 4340 was chosen as a typical notch-sensitive high-strength steel. It was obtained as 1-in diameter round stock of the following composition:

C	Mn	P	S	Si	Ni	Cr	Mo
.39	.77	.012	.015	.30	1.75	.81	.22

All material was received in the spheroidized condition and normalized from 1650°F before being machined into round, circumferentially-notched specimens (Fig. 1). Subsequent heat treatment consisted of austenitizing one hour at 1550°F in argon, oil quenching, refrigerating in liquid nitrogen (-320°F) within 15 minutes of quenching, and tempering one hour in a circulating air furnace.

Two special precautions were taken to reduce scatter in the measurements of plane-strain fracture toughness (Appendix A): (1) the tips of the machined notches were sharpened by the introduction of 0.06-in deep fatigue cracks (well below the approximately 0.002-in deep decarburized surface layer), and (2) a special loading fixture designed to reduce bending was used when the estimated fracture load was below 50,000 lbs. ($G_{IC} < 150$ in-lb/in^2). All other specimens were tested using a conventional ball-and-socket assembly. From the surface of the fractured specimens, the average diameter of the section remaining after fatigue cracking, d, was obtained by measurement with a divider and scale. For purposes of calculating fracture toughness, it was assumed that no slow crack growth occurred. Data are listed in Table I. Also included in Table I are tensile data on quenched and tempered AISI 4340 steel from the Shih, et al (14). There were no tests on unnotched specimens in the present work. Such tests were eliminated in favor of the detailed results from Shih, et al because steel composition and tempering characteristics were essentially the same in that work and this.

The plane-strain fracture toughness, G_{IC}, was calculated with the expression obtained by Bueckner and cited by Wundt(10) for round circumferentially-notched tensile bars:

$$G_{Ic} = \frac{1-\nu^2}{E}\,\sigma_N^2\, d\, f\left(\frac{d}{D}\right) \tag{3}$$

where

σ_N = mean (net-section) stress over the minimum section, calculated from the fracture load and a value of d

d = the diameter of the net section (remaining after fatigue cracking)

D = the major diameter of the specimen (prior to notching)

ν = Poisson's ratio (taken as 0.3)

E = Young's modulus (taken as 29×10^6 psi)

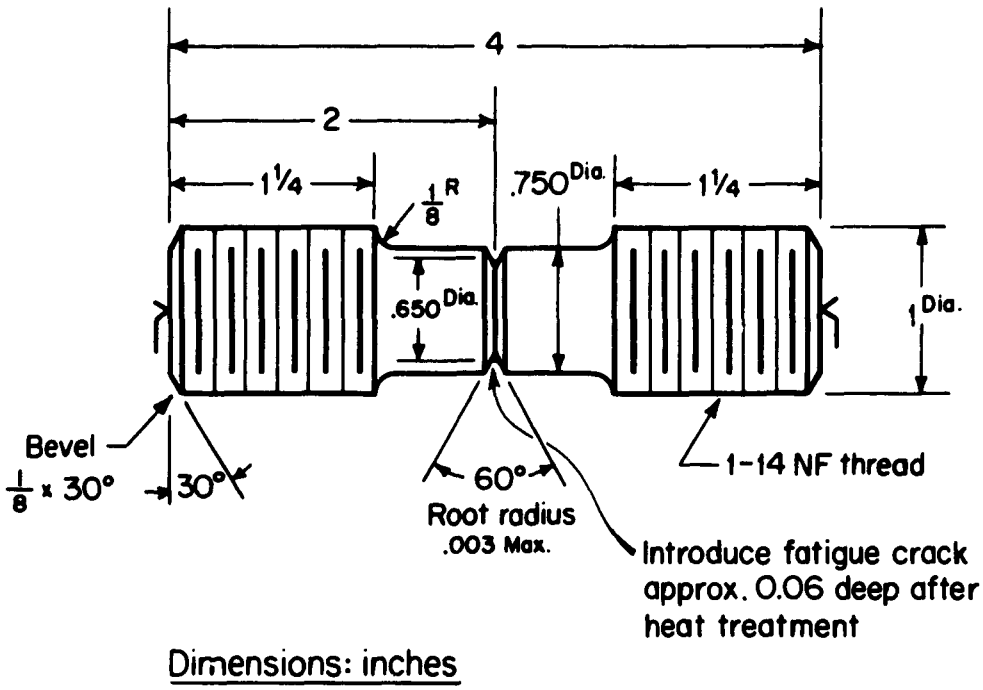

Figure 1 - Circumferentially notched tensile specimen for plane-strain fracture toughness measurements.

TABLE I

FRACTURE DATA

Specimen Number	Tempering Temperature °F	Hardness, R_c	Fracture Load, lbs.	d inches+	σ_N psi	G_{IC} in-lb/in^2	K_{IC} psi $\sqrt{in}$	σ_y psi++	σ_N/σ_y
E-2	RT	58.0	7,900	.575	30,500	4.4	11,900	180,000	.17
E-3	212	57.5	8.460	.570	33,100	5.3	13,000	221,000	.15
E-4	212	58.0	7.960	.540	34,800	5.9	13,800	221,000	.16
E-18	250	57.5	11,850	.575	45,500	9.9	17,800	228,000	.20
E-5	300	57.5	13,300	.525	61,400	18.6	24,400	232,000	.26
E-6	300	57.5	13,300	.525	59,100	17.1	23,400	232,000	.25
E-7	400	57.5	13,200	.500	67,300	22.2	26,700	238,000	.28
E-8	400	56.5	14,600	.515	70,000	24.1	27,800	238,000	.29
E-19	500	53.0	21,700	.525	100,000	47.5	39,000	236,000	.42
E-20	500	53.5	20,350	.505	101,000	50.0	40,000	236,000	.43
E-11	600	51.5	22,400	.490	119,000	69.0	47,000	229,000	.52
E-12	600	51.5	39,600	.630	127,000	68.5	46,800	229,000	.55
E-21	700	50.0	34,150	.530	15[illegible],000	118	61,500	217,000	.71
E-22	700	50.0	35,450	.565	141,000	96.3	55,500	217,000	.65
E-9	800	47.5	60,800	.563	244,000	288	96,000	200,000	1.22
E-10	800	47.5	39,900	.490	212,000	220	84,000	200,000	1.06
E-13	1000	39.0	63,100	.555	261,000	332	103,000	165,000	1.57
E-14	1000	39.0	59,700	.535	266,000	345	105,000	165,000	1.60
E-15	1200	30.0	53,700	.590	196,000	179	75,700	126,000	1.55
E-16	1200	31.0	54,000	.590	197,000	181	76,000	126,000	1.55
E-24	1200	31.0	46,100	.492	243,000	290	96,300	126,000	1.95

+ Major diameter D = 0.75 in. (see Fig. 1).
++ Taken from data of Shih, Averbach, and Cohen(14).

The function f(d/D), a geometric factor which compensates for variation in the ratio (d/D), is given by

$$f\left(\frac{d}{D}\right) = \frac{8\pi\left[1-\left(\frac{d}{D}\right)^2\right]}{\left\{5+3\left[1-\left(\frac{d}{D}\right)^2\right]\right\}^2} \tag{4}$$

The alternative measure of plane-strain fracture toughness, K_{IC}, was calculated from:

$$K_{Ic} = \sqrt{\frac{E G_{Ic}}{1-\mu^2}} \tag{5}$$

Clearly, whichever parameter is mentioned later in the text, the other is also implied.

Equations 3 and 5 are applicable to a good degree of approximation when fracture occurs prior to general yielding. If a specimen yields throughout before fracture, error is introduced in the calculated G_{IC} and K_{IC}. The error increases in the direction of underestimating fracture toughness as (σ_N/σ_Y), where σ_Y is unnotched yield strength, becomes larger than the "critical" value for yielding over the full cross section.

To determine this limiting value of (σ_N/σ_Y), several tests were made under conditions selected to insure general yielding. Circumferentially notched specimens of 0.20-in major diameter, but geometrically similar to the others, were quenched and tempered at 1200°F before being fatigue cracked to various depths. Owing to the small size and high tempering temperature, yield-point drops were evident in tensile load-elongation records and these could be identified with the onset of full yielding. The associated (σ_N/σ_Y) was variable with the depth of notching being about 1.5 for a half-area notch. Therefore, it was concluded that as long as fracture occurred at $(\sigma_N/\sigma_Y) < 1.5$ the plastic zone could be viewed as confined around the crack tip, as required for proper use of Eqs. 3 and 5. According to data in Table I, all measurements after tempering at 800°F or below are free of the error under discussion.

In the over-all program, measurements of G_{IC} (or K_{IC}) were made at room temperature for selected tempering temperatures between room temperature (as-quenched and refrigerated) and 1200°F. At least two specimens were tested for any particular tempering temperature. In one case, twelve specimens were tested after tempering at 400°F, and from these data it could be concluded that the average of measurements in two tests was within $\pm$ 10% of that obtained by breaking the larger number of specimens.

With the results of sectioning experiments described later, it was further estimated that the error in K_{IC} from disregarding any stable (slow) crack growth was 5% or less for material tempered at or below 800°F. After tempering above 800°F, the ratio σ_N/σ_y was greater than 1.5 so that errors resulting from a condition of full plasticity probably outweighed those introduced by ignoring stable crack growth.

As shown in Table I and Fig. 2, K_{IC} increased steadily with tempering temperature with no indication of a "500°F embrittlement". Also included in Fig. 2 are K_{IC} values calculated from data on circumferentially-notched specimens with notch-root radii of 0.001-in(15) and K_c values from edge-notched 0.1-in thick sheet(16). The importance of using fatigue-crack sharpened notches is apparent; compared to a notch of 0.001-in radius, a fatigue-cracked notch acted to reduce K_{IC} by a factor of 3 for material tempered at 400°F. Comparison of the sheet (plane stress) and plane-strain fracture toughness illustrates two important distinctions between K_c and K_{IC} in AISI 4340 steel. First, K_c is much larger at all tempering temperatures. Also, even though shear constituted less than 15% of the fracture surface in sheet specimens tempered below 200°F, K_c was still more than twice K_{IC}. Clearly, the implication is that much more energy is absorbed in shear than in the flat-fracture mode.

The topographical detail of the fractures was considerably coarser for the higher tempering temperatures, which is evident in the fractographs of Fig. 3. Two other typical fracture details are the "focus" and the "crescent", further illustrated schematically in Fig. 4a. Radial lines converge at the focus, as in Figs. 3a-c, or the surface pattern is centered around it as in Fig. 3d. The crescent lies next to the fatigue crack and its maximum width occurs diametrically opposite the focus. Circumferential markings appear within the crescent-shaped area, an example being given in Fig. 5a. Such an area could be seen at about 10X in specimens tempered at 700°F and above, that in the specimen tempered at 700°F being only about "3 ridges" wide.

It would seem that the final, fast fracture started at the center of the crescent and moved radially inwards. Since the crack traveled farthest from its place of origin, the last bit of fracturing would be expected to lie where the focus is found, on a diameter through the origin well beyond the mid-point. Because the crack converged along a non-planar surface, the focus must stand in relief, as it does.

At least part of the crescent developed during stable crack growth. This was apparent from longitudinal sections through specimens loaded until stable cracks formed, but unloaded prior to catastropic fracture. Such sections could be prepared only with specimens tempered at 800 and 1200°F; cracking could not be interrupted after tempering at 400°F. Stopping at the proper load was facilitated by the clicking noises heard in a stethoscope held against the specimen tempered at 800°F and by a drop in load and visible widening of the notch during loading of the specimens tempered at 1200°F.

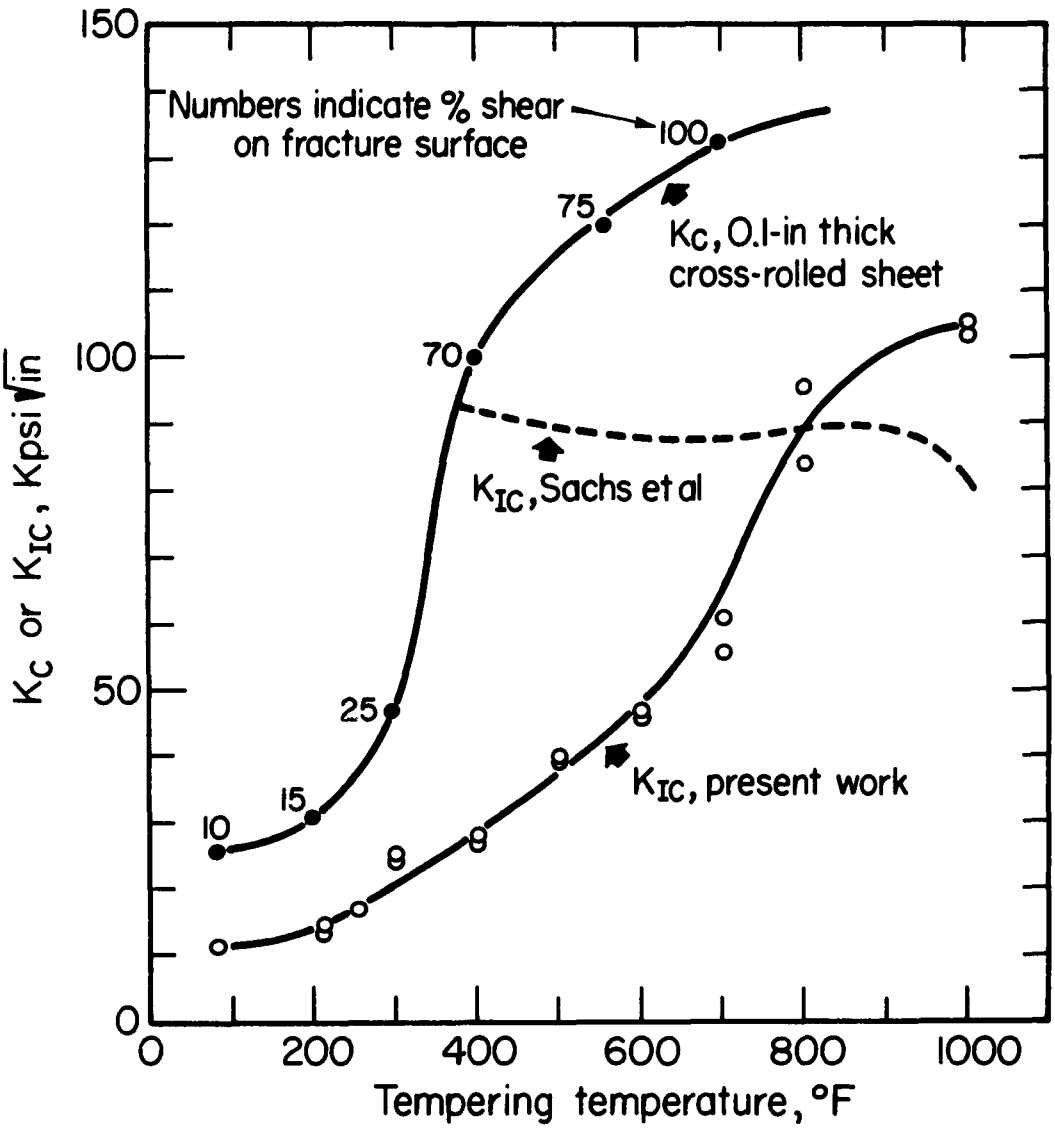

Figure 2 - Fracture toughness of AISI 4340 steel. K_{Ic} values for dull (0.001-in radius) notches calculated from the results of Sachs, et al, as presented in Ref. 15. K_c data from Ref. 16.

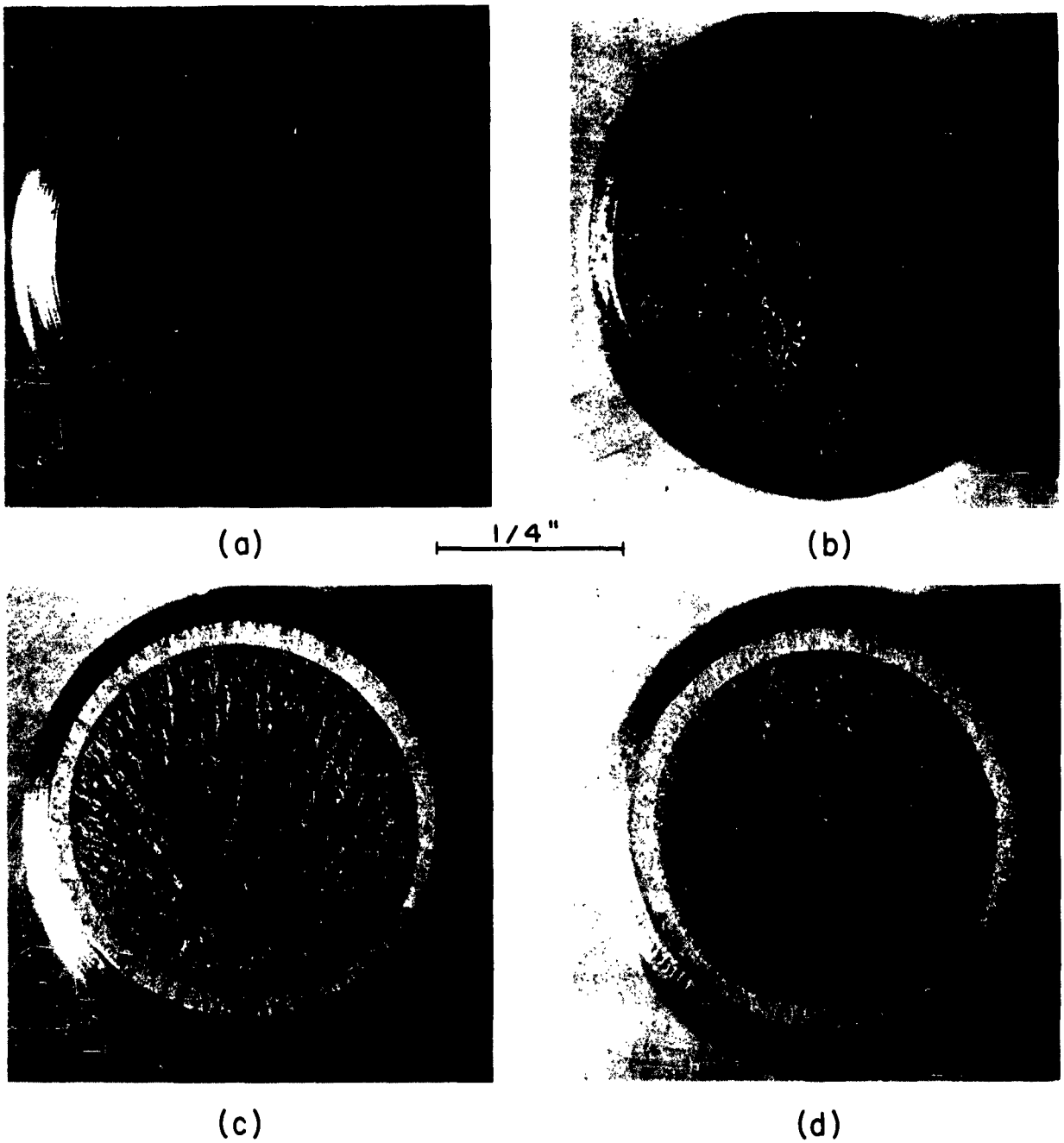

Figure 3 - Typical fracture surfaces. Fatigue crack surface is light, outer band. Tempering temperatures. (a) 400°F, (b) 700°F, (c) 800°F, (d) 1000°F

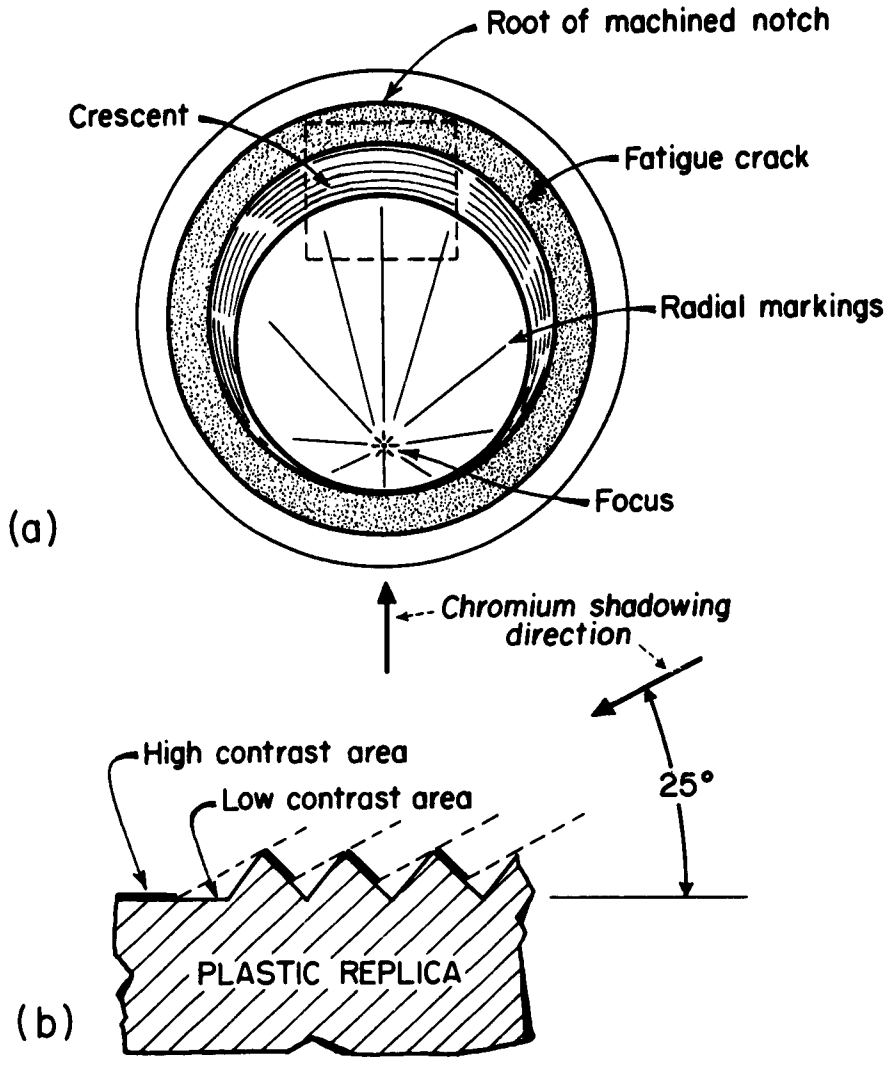

Figrue 4 - Schematic of surface details and chromium-shadowing procedure: (a) general view of the cellulose-acetate replica (area corresponding to the dashed square shown in Fig. 5a); (b) manner of shadowing to develop ridge character of the crescent.

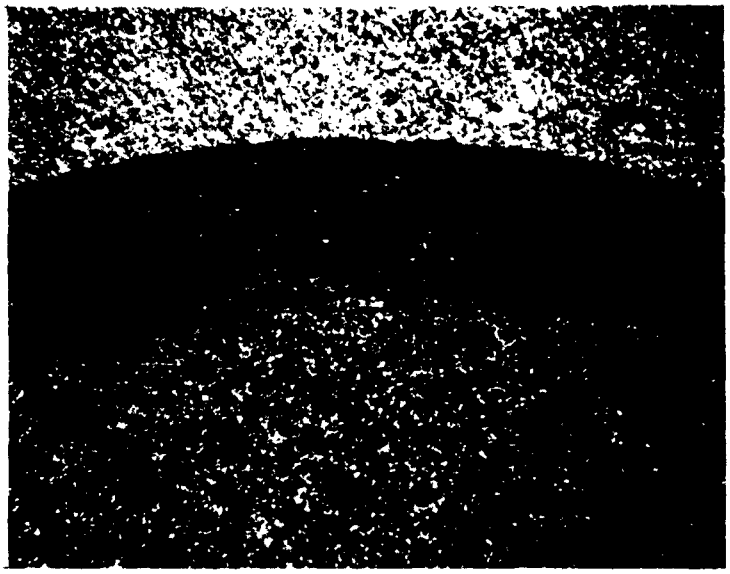

(a)

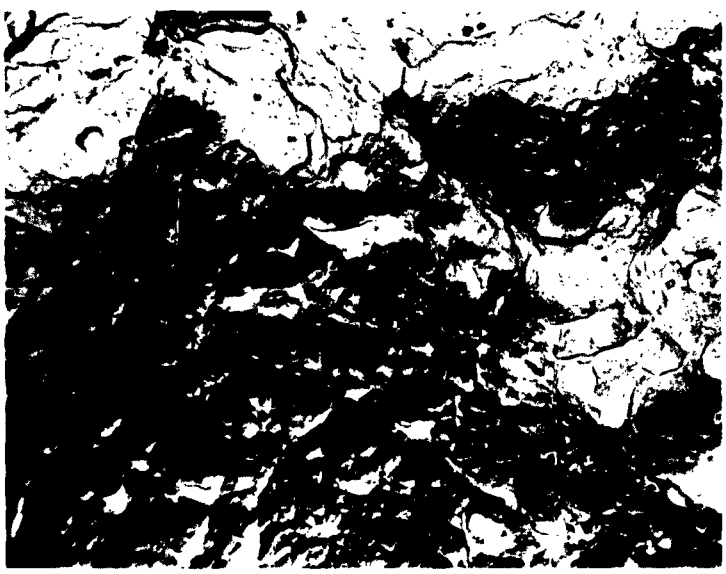

(b)

Figure 5 - Enlarged views of the crescent area.
(a) Macrophotograph. Upper surface is the fatigue crack; lower surface is the radially marked fast fracture region. View corresponds to the dashed square in Fig. 4a. 16X.
(b) Electron micrograph. Boundary across the top of the photograph between high and low contrast areas corresponds to the peak of one circumferential ridge. 4000X.

The ridge-like character of the crescent is indicated in Fig. 6a, a section through a stable crack. The parallel-sided fatigue crack extending from the notch terminates in a stable tensile crack which has intersected an unusually large inclusion. The regular series of inclined and well-matched surfaces is much more evident in Fig. 6b.

To study the process of crescent formation more closely, electron microscopy has also been applied in an examination of the fracture after an 800°F tempering treatment. A two-step negative replica technique was used. The first step involved molding a strip of cellulose acetate against the fracture surface. The second consisted of depositing, by vacuum evaporation, a thin layer of chromium at a small angle to the surface and in a direction at right angles to the ridge structure (Fig. 4); this was followed by a deposit of carbon at nearly normal incidence (replica rotating). Subsequently, the initial replica was dissolved away in acetone, leaving behind the chromium-shadowed negative carbon replica.

Areas exposed to the chromium appear with contrast while those hidden from the deposit do not; in this way the ridged contour of the crescent is made evident. Many areas in the crescent were examined; the view in Fig. 5b is typical. Here the surface has the dimpled appearance characteristic of ductile separation. The light areas appear much the same but without the contrast. Replicas were also prepared from radially-marked areas in specimens tempered at 80, 400 and 800°F. Now the topography was much flatter with an appearance that might be described as a mixture of modes: ductile, intergranular, and cleavage areas all appearing together. The surfaces in Fig. 7 are typical of these regions.

From these observations, tentative conclusions about the fracture sequence may be drawn. In material tempered near 400°F, there is no stable cracking under tensile load and fracture propagates in a mixed mode consisting largely of cleavage. However, after tempering at 800°F and above, a zone of plastic strain is developed at the tip of the fatigue crack. Ductile fracture is responsible for an extension of the crack which accelerates in its advance and propagates unstably in a mixed mode which is predominately ductile. In the latter case, fracture toughness is related to energy absorption when fracture occurs in a ductile mode. Accordingly, it was thought appropriate to consider how ductile fracture might take place under plane strain when the plastic volume is confined around the crack tip.

III. DUCTILE CRACK EXTENSION BY MICROSHEAR

A simple and reasonable description of ductile crack extension under plane strain can be based on a series of local shears within a three-dimensional array of flaws consisting of finely divided inclusions, micropores, etc. The process is pictured schematically in Fig. 8. As load is applied, a thin band of shear extends from the initial crack to a relatively large flaw, as at A. The

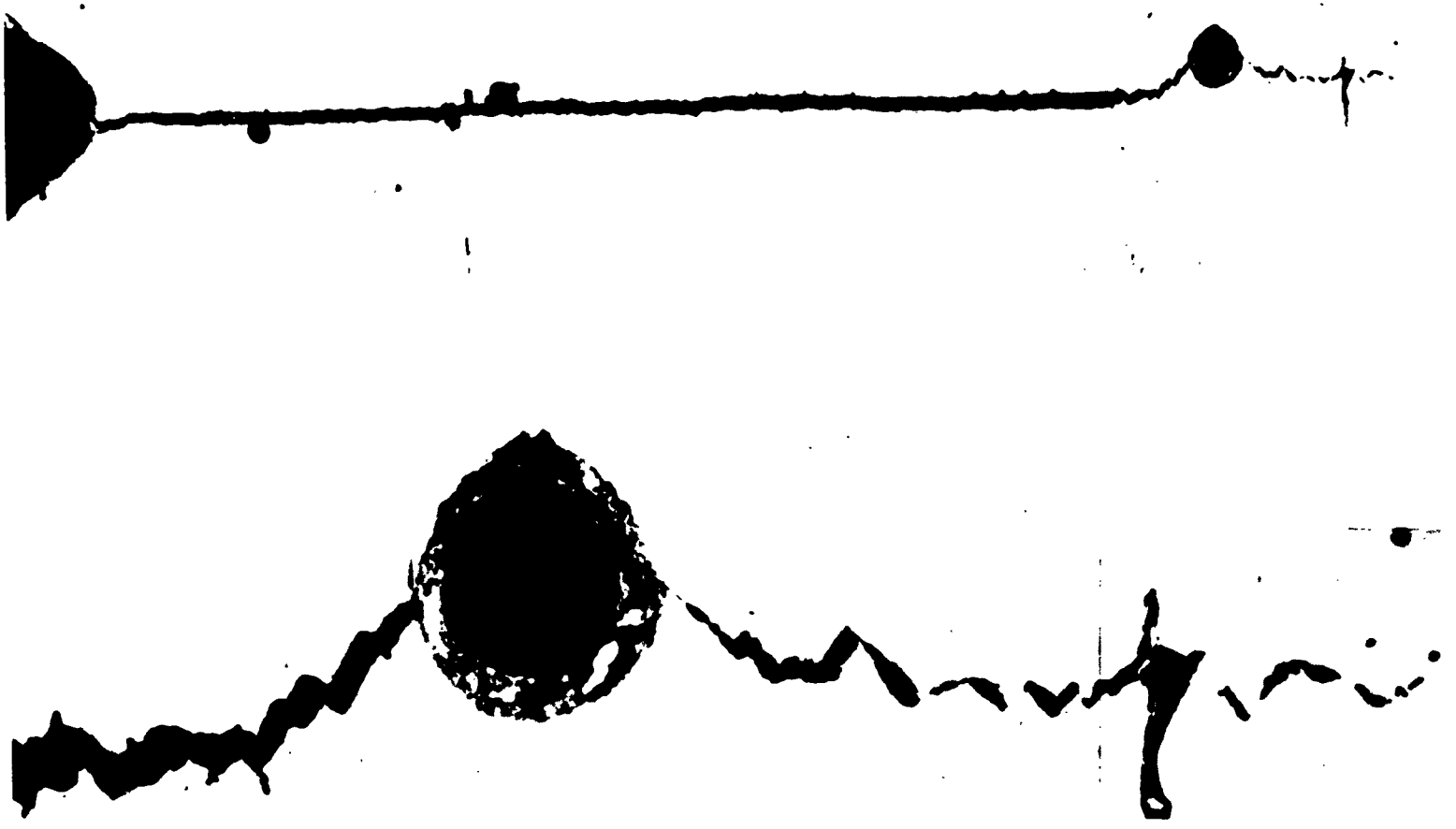

Figure 6 - Longitudinal section along the axis of a specimen tempered at 800°F unloaded and sectioned prior to catastrophic fracture. Unetched. (a) Fatigue crack on the left (parallel sides) beginning at notch root, with stable crack extending through inclusion at the right, 125X. (b) Enlarged view of the stable crack in (a), 700X. Load was applied normal to the fatigue crack.

(a)

(b)

Figure 7 - Examples of fracture topography in radially-marked (unstable fracture) areas.
(a) Specimen as-quenched and refrigerated, 8000X.
(b) Specimen tempered at 800°F after quenching and refrigeration, 14,000X.

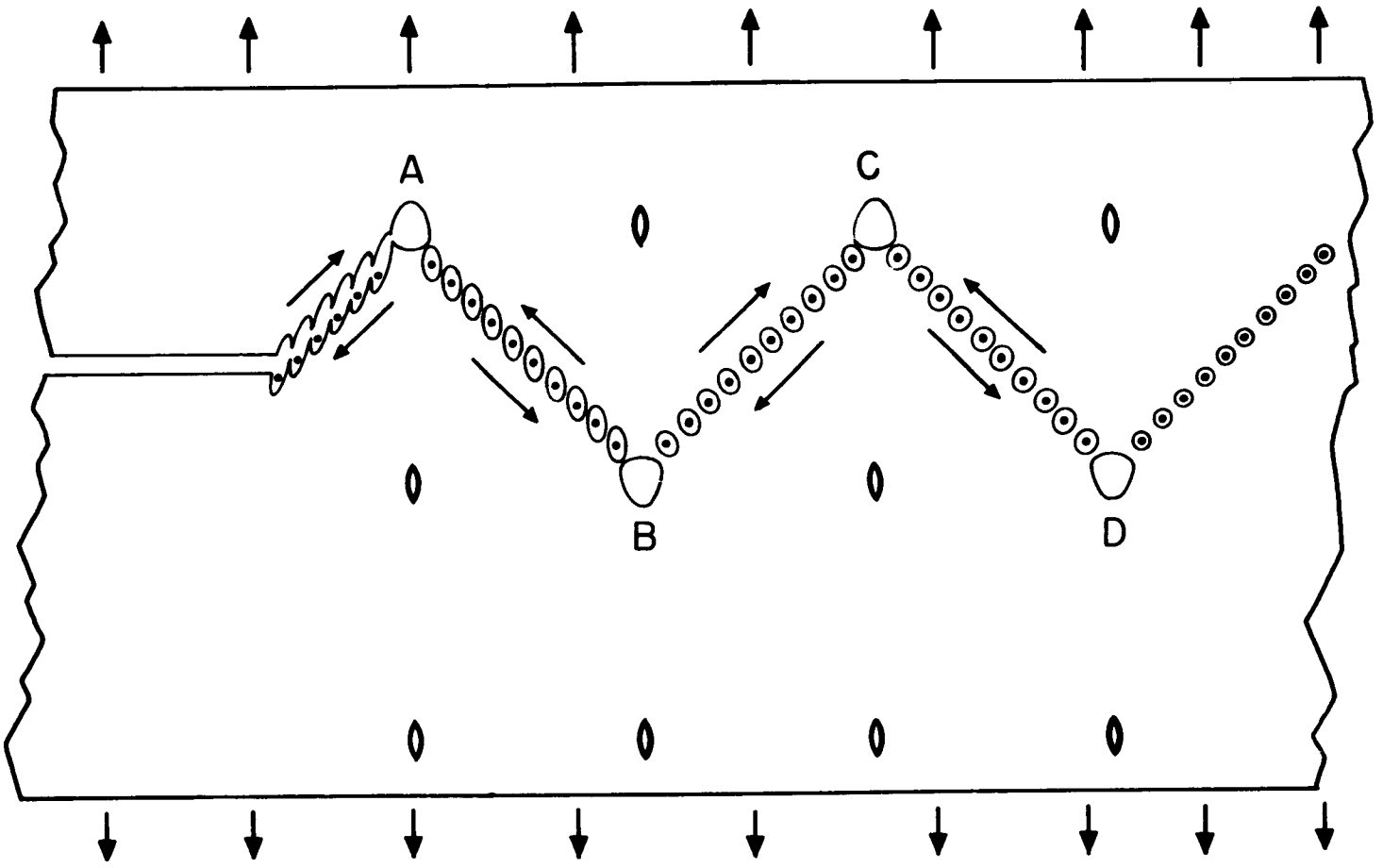

Figure 8 - Schematic representation of ductile fracture by microshearing. Localized shearing has occurred between pre-existent flaws as indicated by displacement arrows. Flaws at the ends of the shear zone change shape and volume to relieve strain concentration. Fracture occurs by a rupturing process to leave a dimpled surface of separation.

penetration of the shear must be restricted by the surrounding elastic material. It would be expected that the presence of such a flaw as at A would aid in relieving concentrations of strain at the end of the band, and may even be necessary for a highly localized shear to develop in the first place. At the same time, tension stress acting across the shear plane ought to contribute to a "void sheet" formation, based in turn on finely dispersed flaws, as considered by Rogers(17) and Crussard(18). With rupturing of ligaments in the void sheet, a crack is formed. Its advance would follow an alternating path A-B, B-C, etc.

Such an elementary model of ductile crack extension invites certain calculations to explore how G_{IC} might be influenced by material characteristics. For purposes of estimating G_{IC}, a relationship based on stress-strain properties and dimensions of the plastic volume can be used.

$$G_{Ic} = -\frac{d W_E}{d A}\bigg|_c = \frac{d W_p}{d A} = \frac{d}{dx}\left[\frac{2 \bar{\sigma} \bar{\epsilon}_p b t_y x}{b}\right] \qquad (6)$$

$$G_{Ic} = 2 \bar{\sigma} \bar{\epsilon}_p t_y \qquad (7)$$

where

W_E = total elastic energy stored in the system

W_p = total plastic work done in extending the crack

$\bar{\sigma}$ = average equivalent stress in the plastic zone at the crack tip

$\bar{\epsilon}_p$ = average equivalent plastic strain in this zone

t_y = the extent of the plastic zone from the crack surface to the point where $\epsilon_p = .002$

x = length of the stable crack

A = area of stable crack

b = unit distance in the width (zero strain) direction

Since G_{IC} is known and $\bar{\sigma}$ can be estimated, it is only necessary to know t_y to calculate a value of $\bar{\epsilon}_p$ from Eq. 7. This may be obtained from an equation given by Irwin(19) for calculating the radius of the plane-strain plastic zone

as fracture becomes unstable

$$t_y = \frac{0.4\ G_{IC}\ E}{2\pi\ (1-\nu^2)\ \sigma_y^2} \tag{8}$$

Equation 8 can be used with values of σ_y and G_{IC} in Table I. The average strain in the zone, $\bar{\epsilon}_p$, can be estimated by combining Eqs. (7) and (8) and taking the value for $\bar{\sigma}$ as the average of the yield and fracture stresses under smooth-bar tensile loading (Table I). Results are given in Table II; $\bar{\epsilon}_p$ is about 0.04, independent of tempering temperature.

Still another estimate, this time of plastic strain at the microshear fracture surface, can be made with some assumption about the gradient of strain normal to the surface. There is no analysis to provide such information, nor have there been any experimental measurements of the gradient in high-strength steel. However, measurements are available of the strain gradients away from a shear-fracture surface in ductile cast iron(20). In that work, fracture was produced by compressing a cylindrical specimen containing a transverse hole; plastic strains were computed from the final shapes of the graphite nodules. Typical results are shown in Fig. 9, where it is clear that the plastic strain decreases nearly exponentially with distance from the fracture surface.

Despite the much higher strength of a heat-treated AISI 4340 steel, the plastic strain gradient in this material might well be of the same form in the neighborhood of a microshear surface as around the macroshear surface on ductile iron. Therefore

$$\epsilon_p = \epsilon_{p(f)}\ e^{[-Bt]} \tag{9}$$

where

ϵ_p = the equivalent plastic strain at any point in the zone

$\epsilon_{p(f)}$ = the value of ϵ_p at the fracture surface (the equivalent plastic strain at fracture)

B = a constant for material of a given thermal-mechanical history

t = a distance normal to the shear fracture surface; t = 0 lies on the surface

TABLE II

PLASTIC STRAINS IN NOTCHED TENSILE SPECIMENS

G_{IC} in-lb/in^2	Tempering Temperature ^oF	σ_y psi (a)	σ_f psi (a)	$\bar{\sigma}$ psi (b)	t_y in. (c)	$\bar{\epsilon}_p$ (d)	$\epsilon_{p(f)}$ (e)
4.5	80	180,000	260,000	220,000	.00029	.036	--
5	180	216,000	290,000	253,000	.00022	.045	--
10	250	228,000	348,000	288,000	.00039	.044	--
25	420	238,000	370,000	304,000	.00090	.045	--
50	510	235,000	349,000	292,000	.00185	.046	--
75	620	227,000	327,000	277,000	.0030	.045	--
100	690	218,000	314,000	266,000	.0043	.044	.20
150	730	212,000	306,000	259,000	.0068	.042	.19
200	760	207,000	303,000	255,000	.0096	.041	.18
250	795	201,000	297,000	249,000	.0125	.039	.17
300	840	193,000	287,000	240,000	.0165	.028	.17

(a) From data of Shih, Averbach and Cohen(14)

(b) $\bar{\sigma} = \frac{1}{2} (\sigma_y + \sigma_f)$

(c) t_y from Eq. (8)

(d) $\bar{\epsilon}_p$ from Eq. (7)

(e) $\epsilon_{p(f)}$ from Eq. (12)

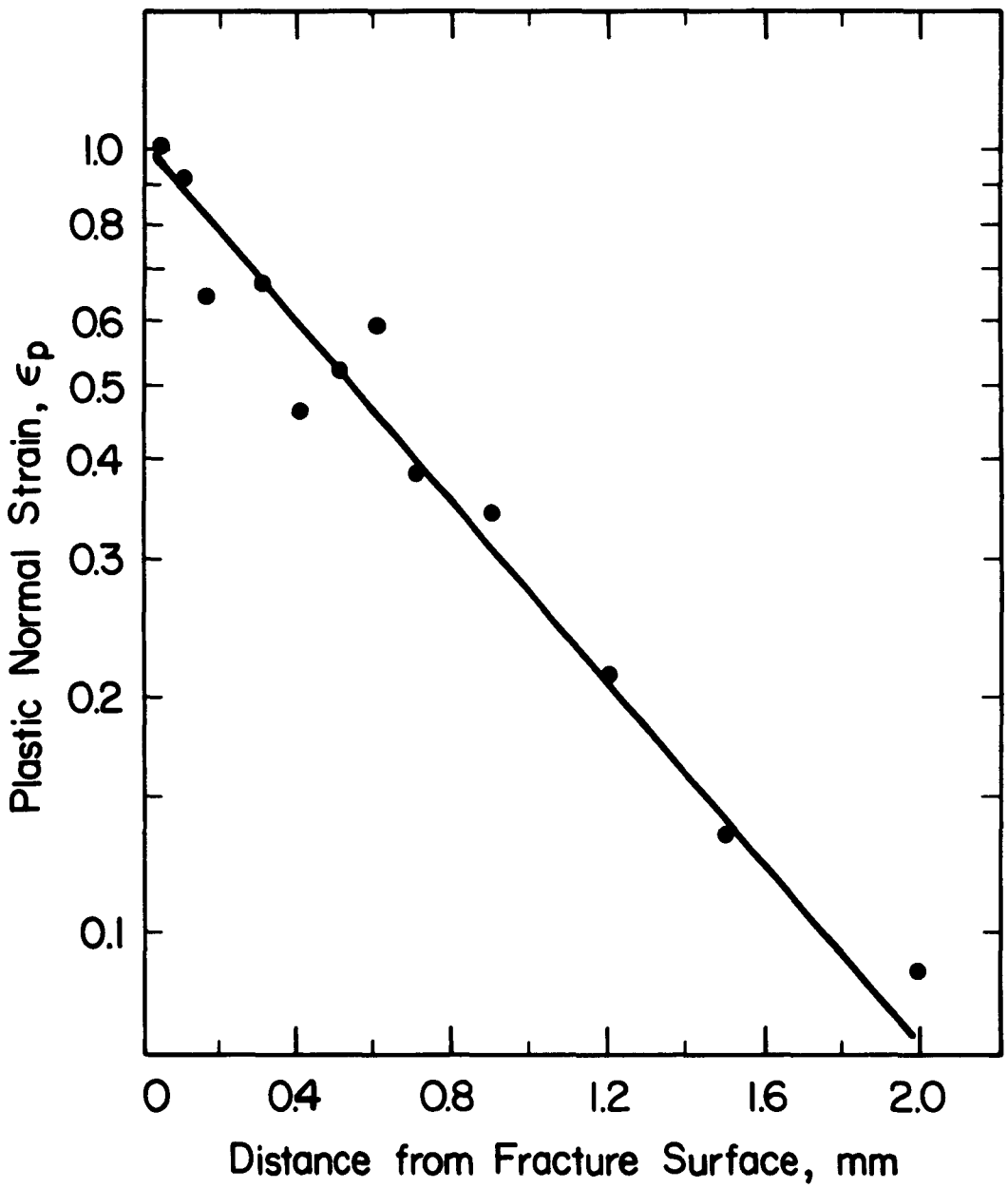

Figure 9 - Variation of plastic strain with distance from a shear fracture surface in ductile cast iron (from Ref. 20).

With exponential decay, the average value, $\bar{\epsilon}_p$, of strain in the range $0 < t < t_y$ is

$$\bar{\epsilon}_p = \frac{\epsilon_{p(f)}}{B\, t_y} \tag{10}$$

if $\epsilon_{p(f)} \gg \epsilon_{p(y)}$ the strain at yielding (0.2%). Combining with Eq. (7),

$$B = \frac{2\bar{\sigma}\,\epsilon_{p(f)}}{G_{Ic}} \tag{11}$$

so that

$$\epsilon_p = \epsilon_{p(f)}\, e^{\left[\frac{-2\bar{\sigma}\epsilon_{p(f)}\, t}{G_{Ic}}\right]} \tag{12}$$

For a given G_{IC} (or tempering temperature), $\epsilon_{p(f)}$ can be obtained by graphical solution of Eq. (12); results are also given in Table II, where only small variations are found in $\epsilon_{p(f)}$. The complete distribution of strain has been plotted for different G_{IC} in Fig. 10. From these calculations, it appears that the average strains in the plastic zone at the crack tip and the strains at the fracture surface change relatively little with temperature of tempering. The implication is that variations in G_{IC} when ductile shear is the significant fracture mode result from variations in the size of the plastic zone.

IV. DISCUSSION

The low values of G_{IC} for material tempered below 700°F are probably the consequence of a non-ductile fracture mode involving cleavage. The elements of microstructure and details of processing history which influence such fracture are still important areas for study. It seems likely, however, that under such conditions patches of cleavage form on arrival of the leading edge of the plastic strain field at the crack tip. Plastic shearing then occurs among these patches producing new crack surface as the high-strain part of the plastic zone passes. For this case the effective fracture

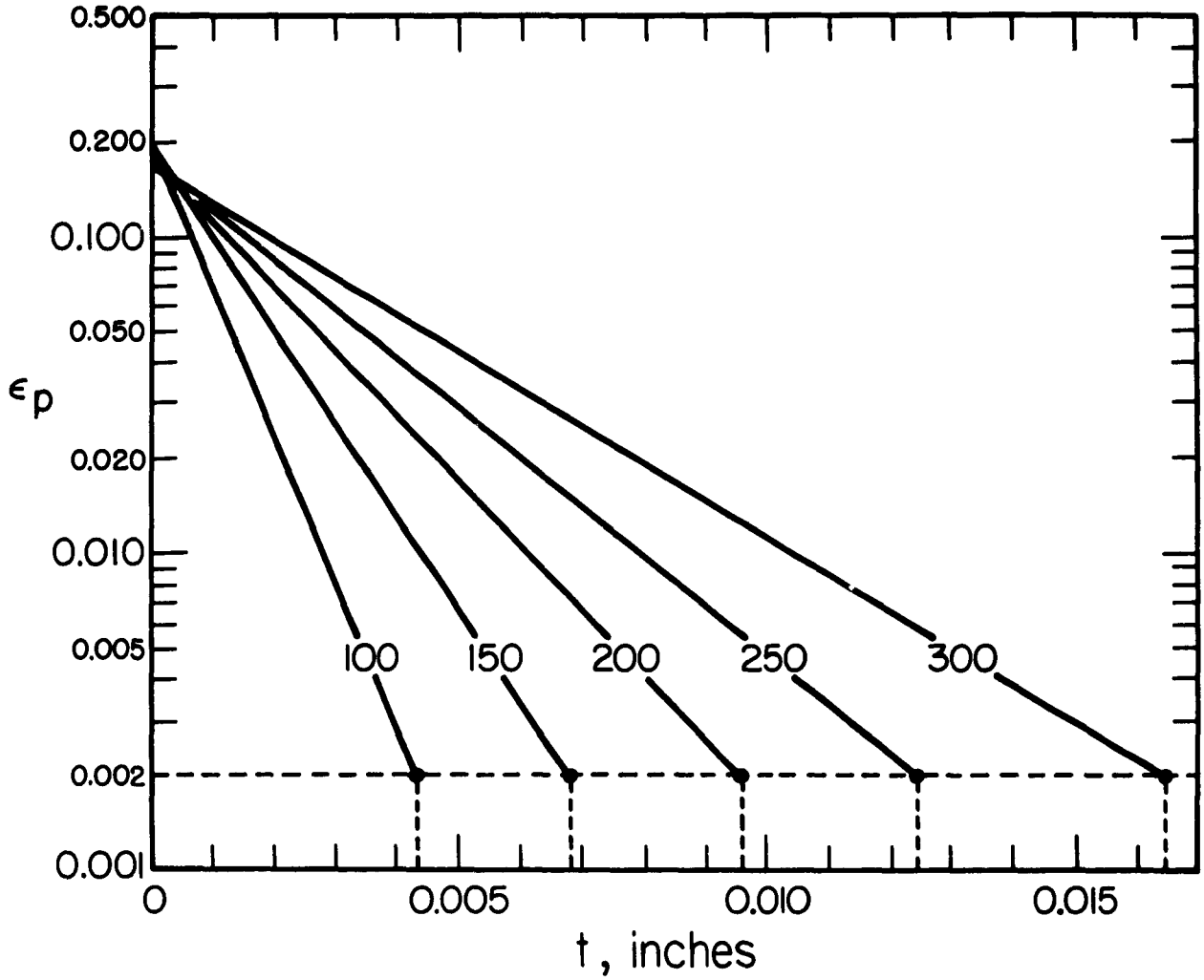

Figure 10 - Estimated plastic strain gradients in predominately ductile plane-strain fractures for several values of G_{IC} (noted on curves). Values of t_y are indicated by dashed vertical lines. All curves represent function of the form of Eq. (12).

toughness, G_{IC}^*, could be considered as an average of that for cleavage fracture, G_{IC} (cleavage), and that for ductile fracture, G_{IC} (ductile).

$$G_{Ic}^{*} = \alpha\, G_{Ic}(\text{cleavage}) + \Phi\, G_{Ic}(\text{ductile}) \tag{13}$$

Since G_{IC} (ductile) $\gg$ G_{IC} (cleavage)

$$\Phi \cong \frac{G_{Ic}^{*}}{G_{Ic}\,(\text{ductile})} \tag{14}$$

Using the data from Table I and assuming fracture after tempering at 1000°F is fully ductile, the proportion of ductile fracture, Φ, would be expected to vary as shown in Fig. 11. As yet no attempt has been made to check this prediction experimentally.

At higher tempering temperatures (above about 800°F) stable crack growth and exclusively ductile fracturing processes would seem to become important in determining the magnitude of G_{IC}. In this context, the observations reported here suggest certain possibilities for controlling the fracture toughness of AISI 4340 steel tempered in this range. The basis rests in processing control.

If G_{IC} is related to fracturing with localized plastic shear, the rather obvious route to higher toughness is an enlargement in the size of the plastic zone and an increase in the maximum plastic strain.

Relative to the zone dimensions, a limiting factor is found in a diminished strain(16) and strain-rate(21) hardening as strength is increased. It is convenient to represent these two important material characteristics, if only approximately, by the exponents in $\sigma/\epsilon = A\epsilon^{n}$ (for strain hardening) and $\sigma/\epsilon = B\dot{\epsilon}^{m}$ (for strain-rate hardening). Both vary more or less together, and their reduction, as by introducing high strength, acts to collapse the plastic volume. Another possible complication with very low strain and strain-rate hardening, even at room temperature, is the onset of adiabatic shear(22). The latter would further restrict the region of flow and aggravate the trend in a direction of notch sensitivity and low fracture toughness.

On the other hand, a possibility for extending the boundaries of a plastic volume exists if the quantity of particles, pores, or other weak interfaces is reduced. In such a way, the mean distance between sites where plasticity can be terminated is enlarged; the size of the volume would be expected to grow and fracture toughness to increase. An

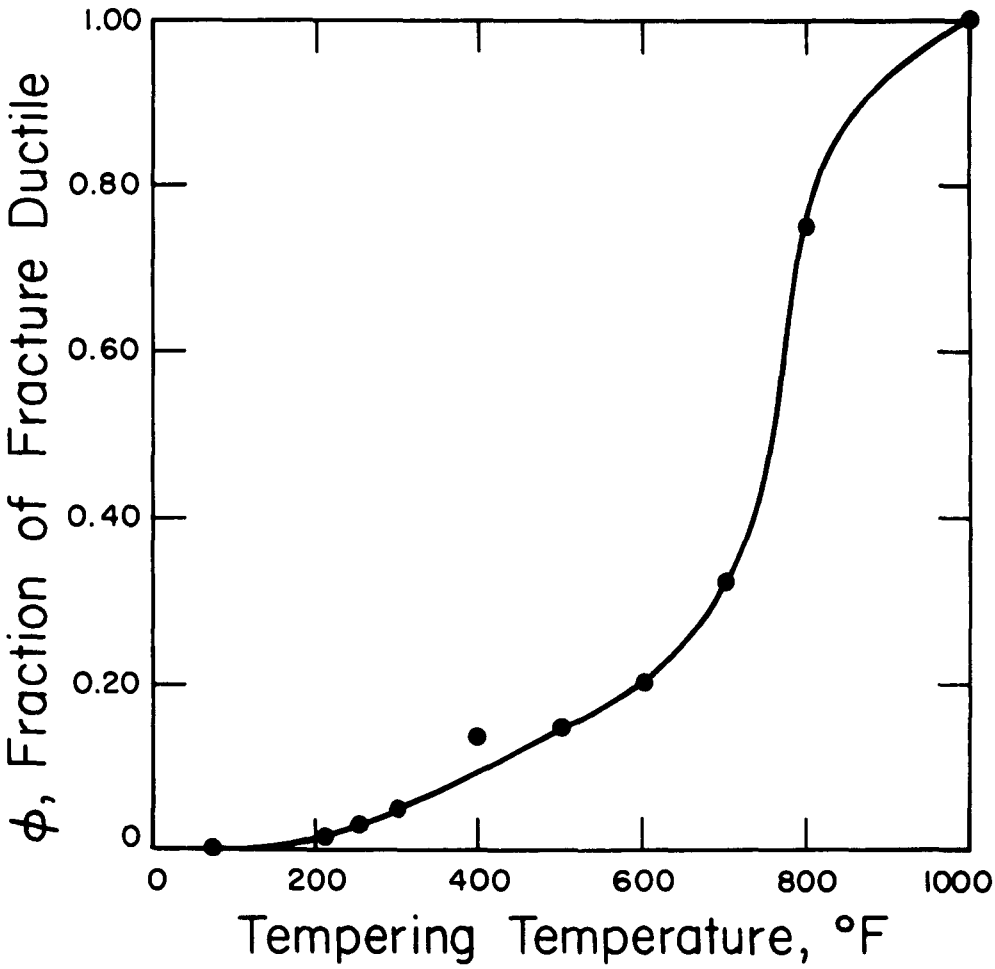

Figure 11 - Approximate fraction of the plane strain fracture surface which is ductile as estimated from Eq. (14).

auxiliary benefit could be anticipated in a larger limit on the shear strain developed within any locally flowing zone; by reducing the number of the various discontinuities it should be possible to accumulate more strain before the region is torn apart.

There is good reason to suspect that any flaw array is closely related to the processing history which provides several opportunities for the introduction of internal surfaces, especially during the solidification of the original ingot. The strong tendency for delamination in the plane of rolling in fractures of heavily rolled sheet specimens(16) is clearly a reflection of "weak" interfaces that may have resulted from loss of cohesion around included particles or an incomplete welding of pore volume by the prior hot working. Thus, control so as to reduce inclusion structure, pore volume, and all such irregularities that may contribute to small-scale volumes with low capacity for plastic-work, ought to give increased G_{IC}.

V. SUMMARY

The plane-strain fracture toughness of quenched and tempered AISI 4340 steel was measured in tension at room temperature with circumferentially-notched and fatigue-cracked specimens. Specific data indicating the range of G_{IC} values encountered were 5.6, 23, and 254 in-lbs/in^2 for tempering temperatures of 212, 400, and 800°F, respectively.

Cracking characteristics were influenced by tempering temperature. Below about 700°F, no stable crack growth was found and propagation occurred by fracture in a mixed mode that appeared to consist partly of cleavage. Between 700 and 1000°F, initial cracking was stable and rapid fracturing again occurred in a mixed mode. After tempering at 1000°F and above, fracture was ductile.

From fractographic studies and estimates of plastic strain, it has been suggested that the basic fracturing process as a crack begins its stable propagation is ductile in nature. A plane-strain ductile fracture process for crack growth is proposed which is imagined to occur by localized plastic shear among a pre-existent array of flaws (inclusions, pore volume, etc.). On the basis of such a model, improvement in toughness under ductile conditions ought to follow from control of material processing history so as to eliminate the flaw structure and thus increase the size and plastic-work capacity of the deforming volume adjacent to the crack.

IV. REFERENCES

1. A. A. Griffith, The Phenomenon of Rupture and Flow in Solids, Philosophical Trans., Royal Society, 1920, Ser. A, 221, p. 163.

2. A. A. Griffith, The Theory of Rupture, Proceedings, First International Congress for Applied Mechanics, 1924, p. 55.

3. E. B. Shand, Fracture Velocity and Fracture Energy of Glass in the Fatigue Range, Journal, American Ceramic Society, 44, 1961, p. 451.

4. E. B. Shand, Correlation of Strength of Glass with Fracture Flaws of Measured Size, Journal, American Ceramic Society, 1961, 44, p. 451.

5. G. R. Irwin, Fracture Dynamics, Fracturing of Metals, ASM, 1948, p. 152.

6. E. Orowan, Fundamentals of Brittle Behaviour in Metals, Fatigue and Fracture of Metals, Ed: W. M. Murray, John Wiley and Sons, 1950.

7. G. R. Irwin, Analysis of Stresses and Strains Near the End of a Crack Traversing a Plate, Journal of Applied Mechanics, transactions of ASME, 1957, 79, p. 361.

8. H. F. Bueckner, The Propagation of Cracks and The Energy of Elastic Deformation, Transactions, ASME, 1958, 80, p. 1225.

9. D. H. Winne and B. M. Wundt, Application of the Griffith-Irwin Theory of Crack Propagation to the Bursting Behaviour of Disks, Including Analytical and Experimental Studies, Transactions, ASME, 1958, 80, p. 1643.

10. B. M. Wundt, A Unified Interpretation of Room-Temperature Strength of Notched Specimens as Influenced by Their Size, ASME Metals Engineering Conference, Albany, 1959, Paper No. 59 MET-9.

11. ASTM Committee on Fracture Testing of High Strength Sheet Material: Report No. 1, Bulletin, ASTM, 1960, p. 29.

12. J. E. Srawley, The Slow Growth and Rapid Propagation of Cracks, NRL Report 5617, May 1961.

13. D. K. Felbeck and E. Orowan, Experiment on Brittle Fracture of Steel Plates, Welding Journal, 1955, 34, Research Supplement, p. 570-S.

14. C. H. Shih, B. L. Averbach and Morris Cohen, Some effects of Silicon on the Mechanical Properties of High Strength Steels, Trans. ASM, 1956, 48, p. 86.

15. G. Sachs, J. D. Lubahn, and L. J. Ebert, Design Properties of High Strength Steels in the Presence of Stress Concentrations - Part I. Tech. Report 56-395, Wright Air Development Center, Aug. 1956, as cited in Materials Research and Standards, March 1962, p. 203.

16. W. A. Backofen and M. L. Ebner, Metallurgical Aspects of Fracture at High Strength Level, Technical Report WAL TR 310.24/5-2, March 1962.

17. H. C. Rogers, The Tensile Fracture of Ductile Metals, AIME, 1960, 218, p. 498.

18. C. Crussard, J. Plateau, R. Tamhander, G. Henry, and D. Lajeunesse, A Comparison of Ductile and Fatigue Fractures, Fracture, Wiley, New York, 1959, p. 524.

19. G. R. Irwin, Plastic Zone near a Crack and Fracture Toughness, Proceedings, 7th Sagamore Ordnance Materials Research Conference, 1960.

20. H. E. Bates, M. L. Ebner, and W. A. Backofen, Shear Fracture in Ductile Iron, to be published.

21. G. I. Taylor, The Testing of Materials at High Rates of Loading, Journal of the Institute of Civil Engineers, 26, 1946, p. 486.

22. W. A. Backofen, Metallurgical Aspects of Ductile Fracture, ASM Conference on Fracture of Engineering Materials, Rensselaer Polytechnic Institute, Troy, New York, August, 1959, to be published.

ACKNOWLEDGEMENTS

The valuable assistance of Dale A. Meyn and Pieter F. S. Bodenstein is gratefully acknowledged.

APPENDIX A

MEASUREMENT OF K_{IC} WITH CIRCUMFERENTIALLY NOTCHED TENSILE SPECIMENS

Recently the measurement of plane strain fracture toughness (K_{IC}) has attracted considerable attention, in part because it is relatively easy to measure in an unambiguous fashion. The most attractive method for obtaining K_{IC} data is the circumferentially notched tensile test. This test has three major advantages: (1) K_{IC} is obtained directly without correcting for a shear-lip contribution, (2) relatively small specimens may be used, and (3) machined notches can be readily sharpened with fatigue cracks.

The size of specimen appropriate to a given set of testing conditions can be determined from a nomograph such as Fig. A-1. In this graph the expression $K_{IC} = \sigma_N \sqrt{d}\, f(d/D)$ (symbols defined in the main report) is plotted in relation to σ_N for constant values of D assuming all specimens contain a half-area notch. K_{IC} is obtained to a good degree of approximation when fracture occurs prior to general yielding ($\sigma_N < 1.5\sigma_y$), so that a conservative procedure is to require $\sigma_N < \sigma_y$. Thus, if a steel with σ_y = 240,000 psi (horizontal dotted line in Fig. A-1) is to be tested at a toughness (K_{IC}) of up to 100,000 psi$\sqrt{\text{in.}}$ (vertical dotted line in Fig. A-1), it is evident that D = 1 in. would be about the smallest appropriate diameter if fracture is to occur at a value of $\sigma_N < \sigma_y$.

A sharp notch is essential when making K_{IC} measurements, and the introduction of a fatigue crack at the notch root is the generally preferred method of sharpening notches. Such cracks can be produced in circumferentially-notched tensile specimens using an ordinary lathe. In the present work, a fatigue crack was introduced at the base of the notch after the specimen (Fig. 1) had been fully machined and heat treated. A crack depth of about 0.06-in. was the goal, as such a crack would extend well below any surface decarburization and as it provided the half-area notch. Cracking was accomplished by loading the specimen as a cantilever and rotating it as shown in Fig. A-2. The bearing on the cantilever arm was positioned to run true by adjusting the four-jaw chuck holding the specimen; this produced the same stress amplitude at each point in the notch root as it rotated to the maximum stress position. A push rod, containing a strain gage load cell, was mounted in the tool post and pressed against the bearing. The force and time required for the crack were determined by trial and error; typical conditions of AISI 4340 tempered at 400°F were lathe speed of 525 RPM for 18 minutes with a force of 160 pounds. (See Ref. 23 for alternative methods of fatigue cracking.)

The fatigue-cracked specimen was loaded to fracture in a special tensile fixture, pictured in Fig. A-3, designed to reduce bending. The sensing elements were two differential-capacitor gages which produce an unbalance signal only when the top of the specimen tilts with respect to the bottom. The circuitry for the

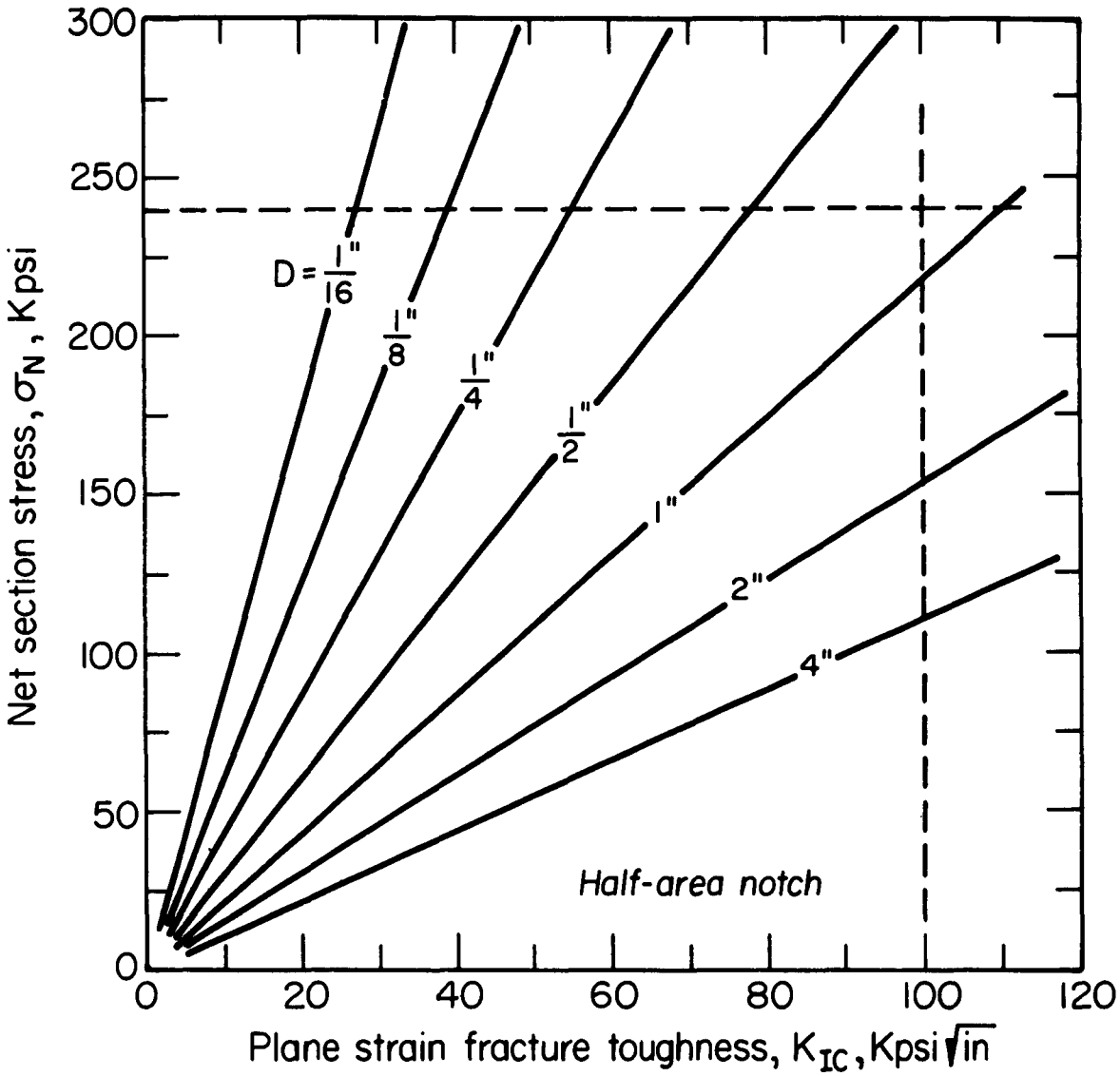

Figure A-1 - Nomograph for determining the appropriate size of circumferentially notched tensile specimens. Major diameter (D, inches) indicated on each curve.

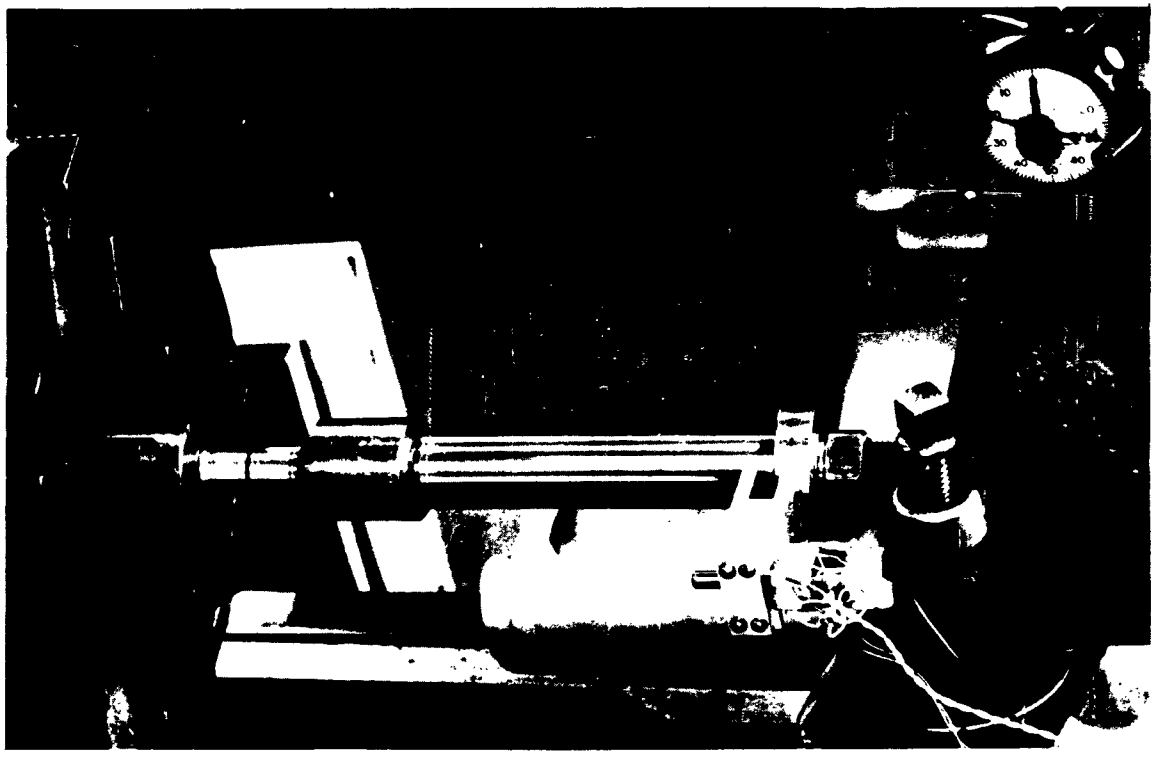

Figure A-2 - Set-up for producing small fatigue cracks at premachined notch in round tensile specimens. Assembly (l. to r.) 4-jaw chuck, split-ring adaptor, specimen, extension arm, bearing, and load cell in tool post.

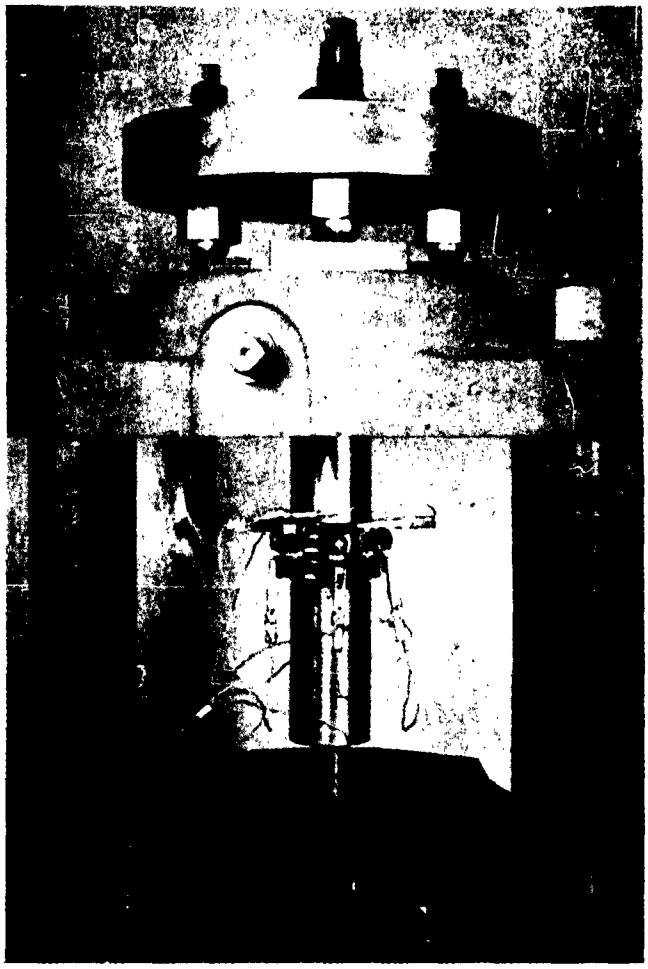

Figure A-3 - Test assembly for loading circumferentially-notched and fatigue-cracked tensile specimens without bending. Adjustable pulling plate at top, capacitor gage on specimen.

gage (Fig. A-4) consisted of a simple bridge, an oscillator, and a voltmeter. The sensitivity of the capacitor bridge is determined primarily by the closeness of the plates (or absolute capacitance), which in turn depends on machining accuracy. After the gages were made, the sensitivity was maximized by adjusting the oscillator frequency for maximum output for a fixed unbalance. For the gages used in the present work it was estimated that a tilt of about 0.02^{o} could be detected.

In a typical test, both gages were balanced before loading and then the specimen was loaded to 25% of the anticipated fracture level. Bending along the specimen was eliminated by adjusting the appropriate screws in the pulling plate until the two capacitor gages indicated no bending in two perpendicular planes containing the specimen axis. Such an adjustment effectively moved the loading axis until it passed through the center of the net section. The capacitor gages were then removed and the specimen loaded to fracture. It was assumed that any additional bending produced between 25 and 100% of the fracture load was negligible.

In Table A-I, K_{IC} obtained according to the above procedure is compared with that determined by using a standard ball-and-socket pulling assembly for the case of AISI 4340 steel austenitized at $1550^{o}F$, oil quenched, refrigerated in liquid nitrogen, and tempered at $400^{o}F$. The different mean values indicate that bending stresses reduce the average K_{IC} value only slightly, particularly for the larger specimens, but that the number of specimens required to estimate K_{IC} may be smaller using the fixture. At higher hardness (lower toughness) levels, the test procedure described here would be expected to have still further value in isolating loading effects on K_{IC}. As a practical matter, however, it seems much more important that the notches be sharpened with fatigue cracks than that the specimen be pulled with a special fixture designed to reduce bending.

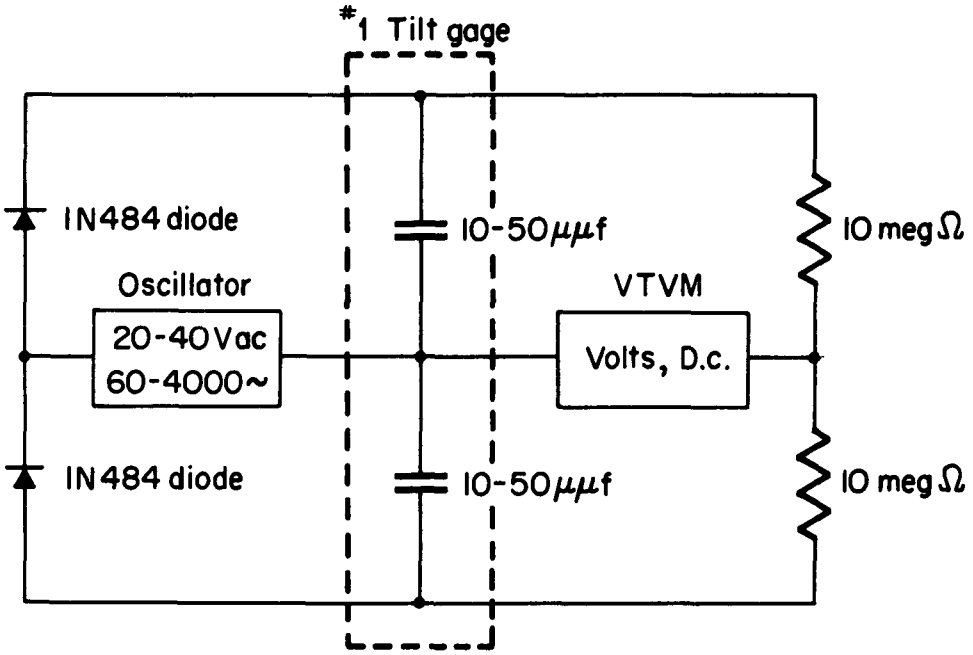

Figure A-4 - Bridge circuit used with the differential capacitor gages shown in Fig. A-3. Oscillator frequency adjusted to give maximum output for a fixed unbalance. No. 2 tilt gage switched into measuring circuit after No. 1 gage is balanced.

TABLE A-I

K_{IC} FOR HARDENED AISI 4340 TEMPERED AT 400°F

With Pulling Fixture		With Ball and Socket	
Specimen	K_{IC} (1)	Specimen	K_{IC} (1)
Major Diameter 0.750 Approx. 1/2 Area Notch, 1 hour temper			
A-2	33,000	A-5	32,400
A-4	29,400	B-43	28,000
A-6	33,600	B-44	32,200
B-41	33-300	B-45	31,800
B-42	31,000	B-46	26,100
		B-47	30,700
		B-48	30,900
	Avg. K_{IC} = 32,060		Avg. K_{IC} = 30,300
	Range = 4,200 psi $\sqrt{in.}$ = ± 6.5%		Range = 6,100 = ± 10.3%
Major Diameter .540 Approx. 1/2 Area Notch, 2 hour temper			
4	32,500	3	33,500
6	33,000	10	31,400
7	31,500	11	32,500
9	33,100	X	32,200
	Avg. K_{IC} = 32,500		Avg. K_{IC} = 32,400
	Range = 2,600 = ± 4.0%		Range = 2,100 = ± 3.3%

(1) K_{IC} calculated from Eqs. 4 and 5, psi $\sqrt{in.}$

APPENDIX B

FRACTURE TOUGHNESS OF STRAIN AGED AISI 4340 STEEL

It is generally recognized, as discussed in the body of this report, that a decrease in the over-all strain hardening rate may lead to a reduction in plastic-work absorption in ductile fracture. Thus interest arose in the effect on fracture toughness of treatments intended to alter the strain-hardening characteristics at high strength levels. Accordingly, the following experiments were made to measure the plane-strain fracture toughness of AISI 4340 steel after a conventional heat treatment and also after treatment involving an additional strain and age cycle; the latter processing schedule might be expected, if it had any effect, to impair fracture toughness.

The maximum strengthening of austenitized and quenched AISI 4340, as found by Stephenson and Cohen(24) occurred after the following "flow-tempering" sequence: one hour at 400°F followed by a 3 - 4% plastic strain in tension plus a subsequent aging period of one hour at 400°F. In the present experiments, this treatment, with varying plastic strains, was repeated.

Cylindrical (unnotched) tensile specimens (0.540 dia.), machined from 1-in. diameter aircraft-quality AISI 4340 steel rod, were austenitized in argon for one hour at 1550°F, oil quenched, and refrigerated in liquid nitrogen. After tempering for one hour at 400°F in a circulating air furnace, the specimens were water-quenched.

After this initial heat treatment, the specimens were strained plastically in tension by different amounts from 0 to 4%. Final values of plastic strain after unloading were accurately determined with a traveling microscope. Aging treatment consisted of one hour at 400°F. The specimens were then divided into two groups, one for measurement of smooth-bar tensile properties and a second for the notched-bar study.

Unnotched Tensile Specimens: The elastic limit was defined as the stress for a residual plastic strain of 1×10^{-6}, and was obtained with a Tuckerman optical extensometer by applying successively higher loads to a specimen and measuring the residual strain on unloading. No negative residual strains, as reported by Muir et al(25), were found.

Load or stress-elongation curves of the strained and aged steel were characterized by a load maximum at yielding, a drop in load to a relatively constant level, and finally, a gradual decrease in load until fracture. A tensile strength was defined in the usual way with the maximum-load value. For prestrain of 1% or more, the 0.1% offset yield strength and tensile strength were the same. The elastic limit proved to be essentially independent of prestrain. Results are summarized in Fig. B-1.

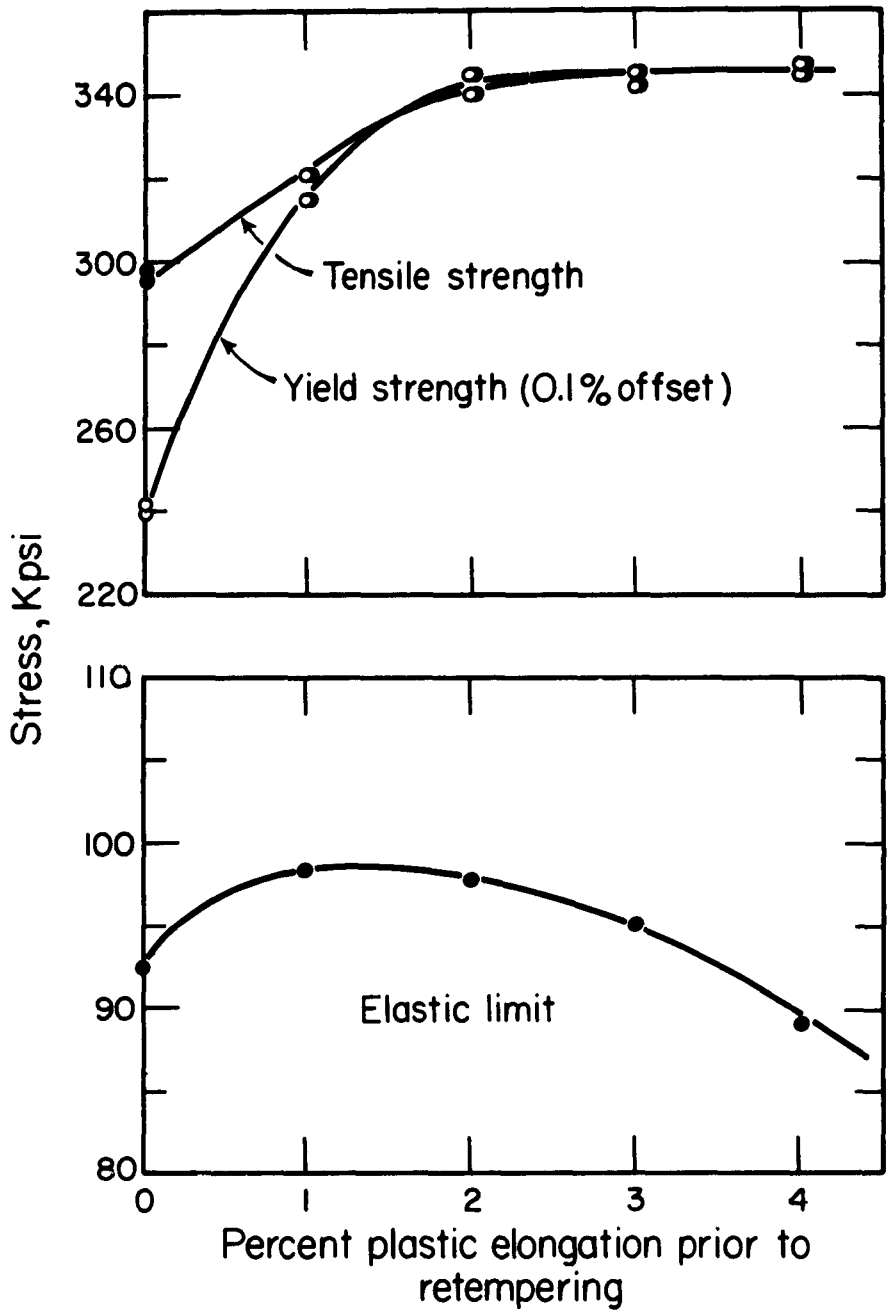

Figure B-1 - Strength of Strain-aged AISI 4340 steel. The elastic limit is the stress at a residual plastic strain of 10^{-6}.

Notched Tensile Specimens: After prestraining and aging, specimens of the second group were notched by grinding followed by fatigue cracking. Testing and K_{IC} evaluation were carried out as described in the body of the report. The main finding was that K_{IC} was effectively constant, within the range 32,000 $\pm$ 2,000 psi $\sqrt{\text{in.}}$, for 13 specimens prestrained different amounts before the final 400°F aging treatment. Thus no impairment in fracture toughness was discovered. The explanation may well be found in relation to the ductility data given in Fig. B-2. Here no particular losses appears in the "local" ductility, reflected in the percentage reduction of area. Some measure of the capacity for distributing plastic strain was obtained from the strain hardening exponent, n, calculated from the yield and fracture values of stress and strain. This exponent was 0.15 for the material without prestrain and .05 for all material which was prestrained. Thus the strain hardening capacity was reduced by prestraining and aging, but from a rather low initial level. Presumably the already limited plastic volumes in plane-strain cracking are not being made any smaller by these treatments.

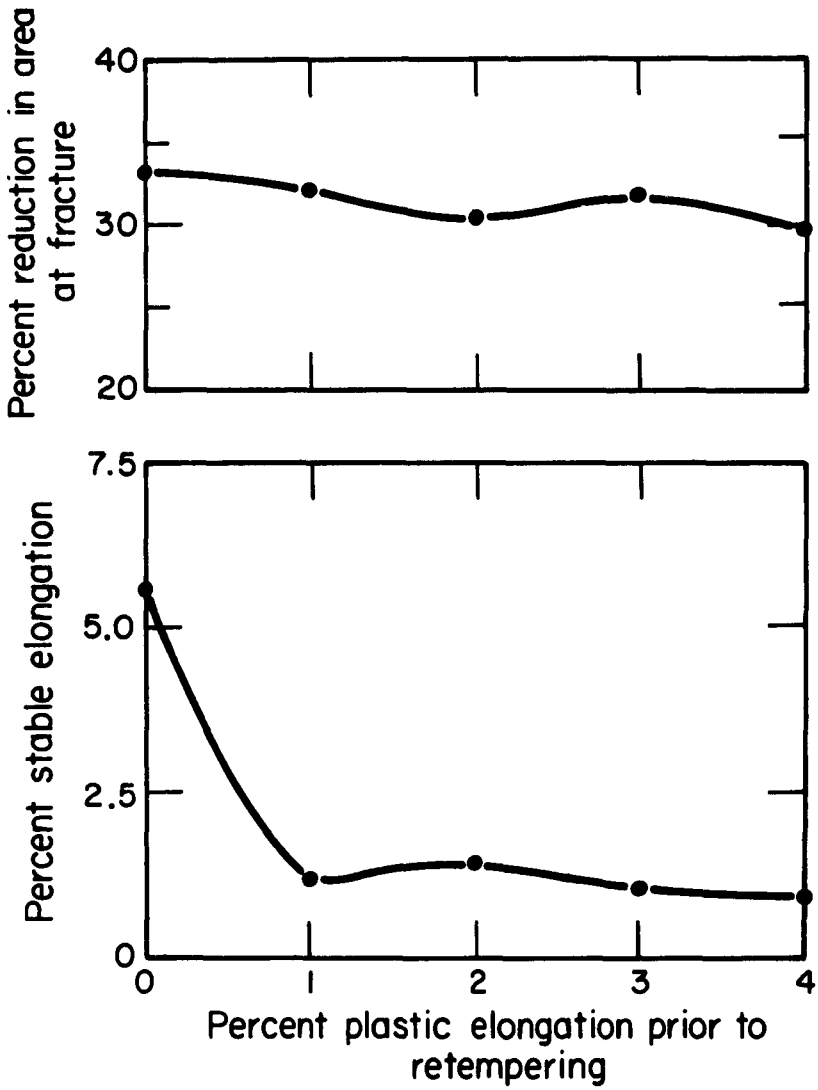

Figure B-2 - Ductility of Strain aged AISI 4340 steel. Stable elongation is that at maximum load.

APPENDIX C

EFFECT OF AUSTENITIZING TEMPERATURE ON FRACTURE TOUGHNESS OF AISI 4340

This study was undertaken as a continuation of prior work(16,26) which indicated that the notch toughness of quenched and tempered AISI 4340 steel apparently increased as the austenitizing temperature was raised.

Circumferentially notched bars of the type shown in Fig. 1 were machined from the as-received rod stock. Heat treatment consisted of austenitizing 1 hour in argon, oil quenching, refrigerating in liquid nitrogen (-320°F) within 15 minutes after quenching, and tempering for one hour at 400°F in a circulating air furnace. All specimens were water quenched from the tempering temperature. Some specimens were given special austenitizing treatments before the final oil quenching, refrigeration and tempering. The hardness after tempering was R_c 54-55 in all cases.

The testing procedure, including fatigue cracking and use of the special pulling fixture (Appendix A), and the method of calculating G_{IC} and K_{IC} were identical with those described earlier.

The fracture data are given in Tables C-I and summarized in Fig. C-1 where G_{IC} is plotted as a function of austenitizing temperature. G_{IC} was increased from 33 to 68 in-lb/in^2 as the austenitizing temperature was raised from 1550 to 2000°F. Austenitizing at still higher temperatures led to much increased scatter. Results with a limited number of special heat treatments are presented in Table C-II. The group I heat-treatments were intended to disclose any effect of prior normalizing, but none was evident in these few tests. Group II heat-treatments were planned so as to isolate any effect of the rate of quenching from the austenite range, but again the variable seemed not to be of much significance.

The prior austenite grain size was measured from photographs of the metallographic sections obtained with polarized light for increased grain contrast. An average grain diameter was computed from an average value of the number of grains/in. intersected by a line through the view; the dependence of austenitizing temperature is shown in Fig. C-2. The plane-strain fracture toughness, G_{IC}, is plotted against grain size in Fig. C-3, and the same trend appears here as in Fig. C-1.

The fracture surface of specimens broken after different austenitizing temperatures are shown in Fig. C-4. Surface roughness has clearly been increased as a result of the austenitizing temperature being raised. Low-power stereomicroscopic examination of specimens austenitized at 2100, 2200, 2250, and 2300°F revealed that intergranular fracture occurred over about 30% of the surface, although there were large variations in this fraction.

TABLE C-1

FRACTURE DATA

Specimen Number	Austenitizing Temperature ^{o}F	Fracture Load lbs.	d inches	σ_N psi	K_{IC} psi $\sqrt{in.}$	G_{IC}	Grain Dia. Inches
A-1	1550	10,000	.557	44,000	17,000	9.0	.0003
A-2	1550	22,300	.585	83,000	33,000	33.9	.0003
A-4	1550	13,200	.476	74,200	29,400	26.8	.0003
A-6	1550	20,300	.552	85,000	33,600	35.2	.0003
B-41	1550	14,000	.457	85,500	33,300	34.5	.0003
B-42	1550	15,300	.500	78,000	31,000	28.8	.0003
B-19*	1550	19,100	.542	82,700	32,700	33.2	.0003
B-43**	1550	12,620	.476	71,000	28,000	24.3	.0003
B-44**	1550	9,850	.378	87,700	32,200	32.2	.0003
B-45**	1550	14,250	.473	81,000	31,800	31.5	.0003
B-46**	1550	10,280	.441	67,600	26,100	21.1	.0003
B-47**	1550	11,600	.429	80,000	30,700	29.3	.0003
B-48**	1550	12,030	.437	80,300	30,900	29.6	.0003
B-22	1750	22,000	.547	93,700	37,000	42.6	.0004
B-23	1750	21,900	.563	88,000	34,700	37.5	.0004
B-24	1750	20,000	.550	84,100	33,300	34.5	.0004
B-10	1800	25,800	.578	98,100	38,200	45.3	.0005
B-20***	1800	11,900	.378	106,000	38,900	47.0	.0005
B-21***	1900	14,500	.445	91,200	35,400	38.9	.0008

All specimens held 1 hour at temperature, oil quenched, refrigerated in liquid nitrogen, air tempered 1 hour at $400^{o}F$.

* Quenched into hot oil ($2000^{o}F$).

** Broken using well-aligned ball and socket fixtures.

*** Retempered 10 minutes at $400^{o}F$ after fatigue cracking to heat-tint fatigue crack surface.

TABLE C-I (continued)

FRACTURE DATA

Specimen Number	Austenitizing Temperature °F	Fracture Load lbs.	d inches	σ_N psi	K_{IC} psi $\sqrt{in.}$	G_{IC}	Grain Dia. Inches
B-25***	1900	10,000	.445	91,200	35,400	38.9	.0008
B-26***	1900	9,200	.375	83,200	31,200	30.2	.0008
B-27***	1900	11,000	.354	111,000	39,700	49.5	.0008
B-4	2000	26,700	.547	114,000	44,500	61.6	.0015
B-13	2000	25,800	.540	112,500	44,700	62.0	.0015
B-17	2000	33,500	.570	131,000	51,600	82.4	.0015
B-38	2000	36,100	.630	116,000	44,300	61.0	.0015
B-39	2000	31,900	.594	116,000	44,400	61.3	.0015
B-5	2100	34,200	.594	124,000	47,400	69.8	.003
B-7	2100	34,200	.609	117,000	45,000	62.8	.003
B-8	2100	33,400	.609	115,000	44,200	60.7	.003
B-9	2100	30,700	.575	118,000	44,800	62.2	.003
B-6	2200	19,700	.54	82,300	32,600	33.0	.009
B-28***	2200	30,100	.543	130,000	51,500	82.5	.009
B-29***	2200	23,900	.526	110,000	43,700	59.2	.009
B-3	2250	14,800	.49	79,000	31,000	29.8	.015
B-2	2300	14,000	.55	59,200	23,300	16.8	.03
B-32	2300	40,100	.59	146,000	56,500	99.0	.03

All specimens held 1 hour at temperature, oil quenched, refrigerated in liquid nitrogen, air tempered 1 hour at 400°F.

*** Retempered 10 minutes at 400°F after fatigue cracking to heat-tint fatigue crack surface.

TABLE C-II

SPECIAL HEAT TREATMENTS

1. Normalized austenitized at 1550°F, oil quenched, refrigerated in liquid nitrogen, tempered one hour at 400°F.

Specimen Number	Normalizing Temperature °F	Fracture Load lbs.	d inches	σ_N psi	K_{IC} psi $\sqrt{in.}$	G_{IC}
B-35	1750	29,400	.614	99,300	38,100	45.1
B-36	1750	22,400	.573	68,000	26,600	22.0
B-15	2100	22,500	.577	86,000	33,400	34.6
B-18	2300	17,300	.570	66,500	26,100	21.2

* Furnace cooled (cooling rate of approximately 50°F/minute) to 1600°F before air cooling.

2. Austenitized one hour at temperature, furnace cooled to 1550°F, oil quenched, refrigerated in liquid nitrogen, tempered one hour at 400°F.

Specimen Number	Normalizing Temperature °F	Fracture Load lbs.	d inches	σ_N psi	K_{IC} psi $\sqrt{in.}$	G_{IC}
B-12	2100	21,300	.563	85,500	33,700	35.3
B-14	2100	23,300	.504	116,500	46,300	66.6
B-33	2100	22,400	.549	94,500	37,400	43.5
B-34	2100	31,500	.588	116,000	44,800	62.4
B-1**	2300	17,200	.42	124,000	47,000	68.5

** Cooling time five hours, quenched from 1750°F.

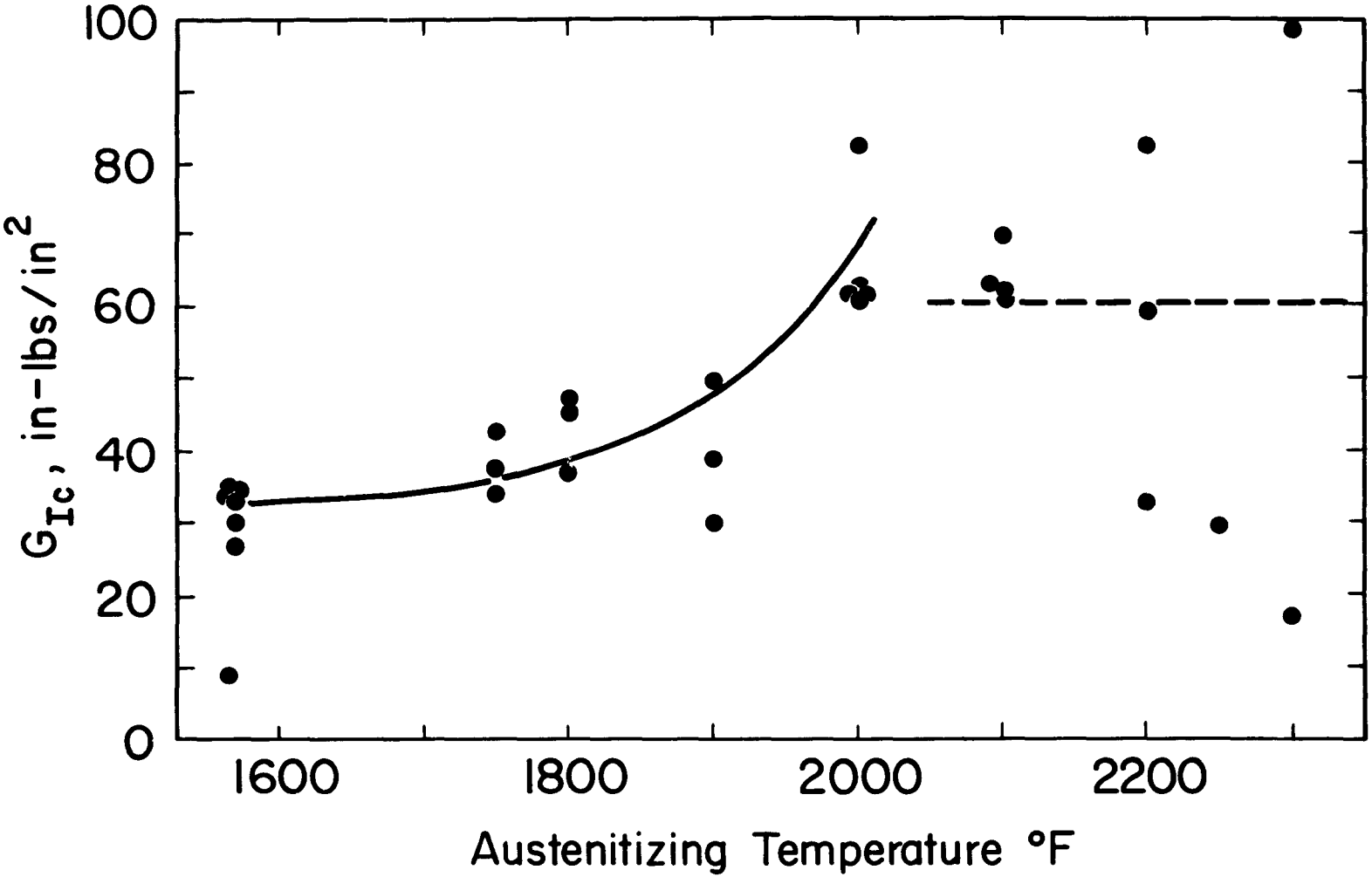

Figure C-1 - Plane strain fracture toughness, G_{IC}, of AISI 4340 steel as a function of the temperature of austenitizing prior to oil quenching, refrigerating in liquid nitrogen and tempering at 400°F.

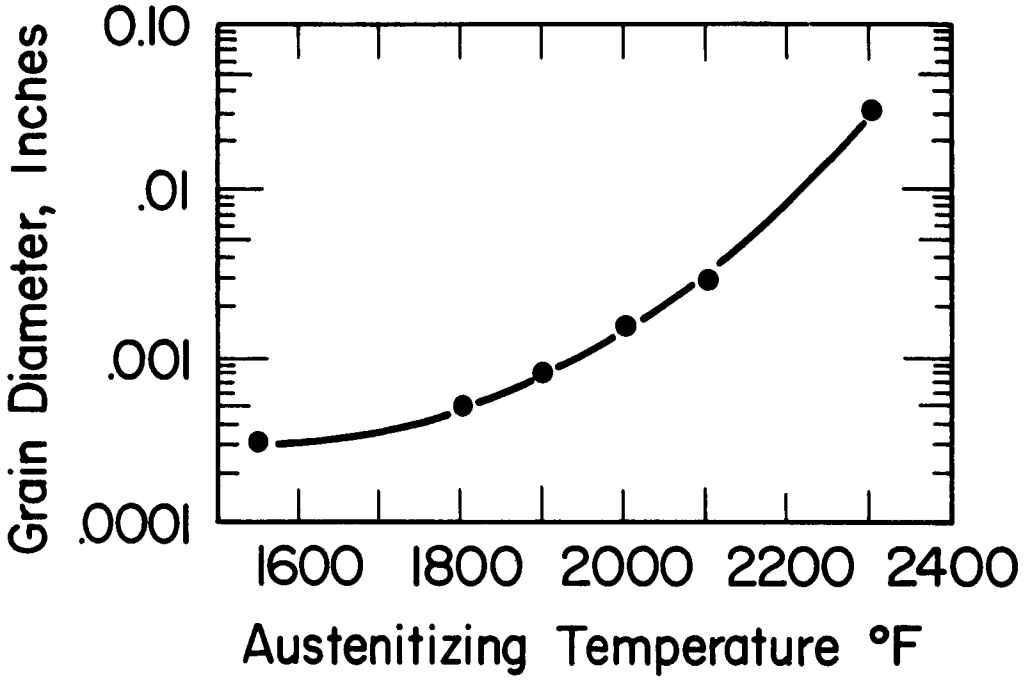

Figure C-2 - Prior austenite grain size as a function of austenitizing temperature.

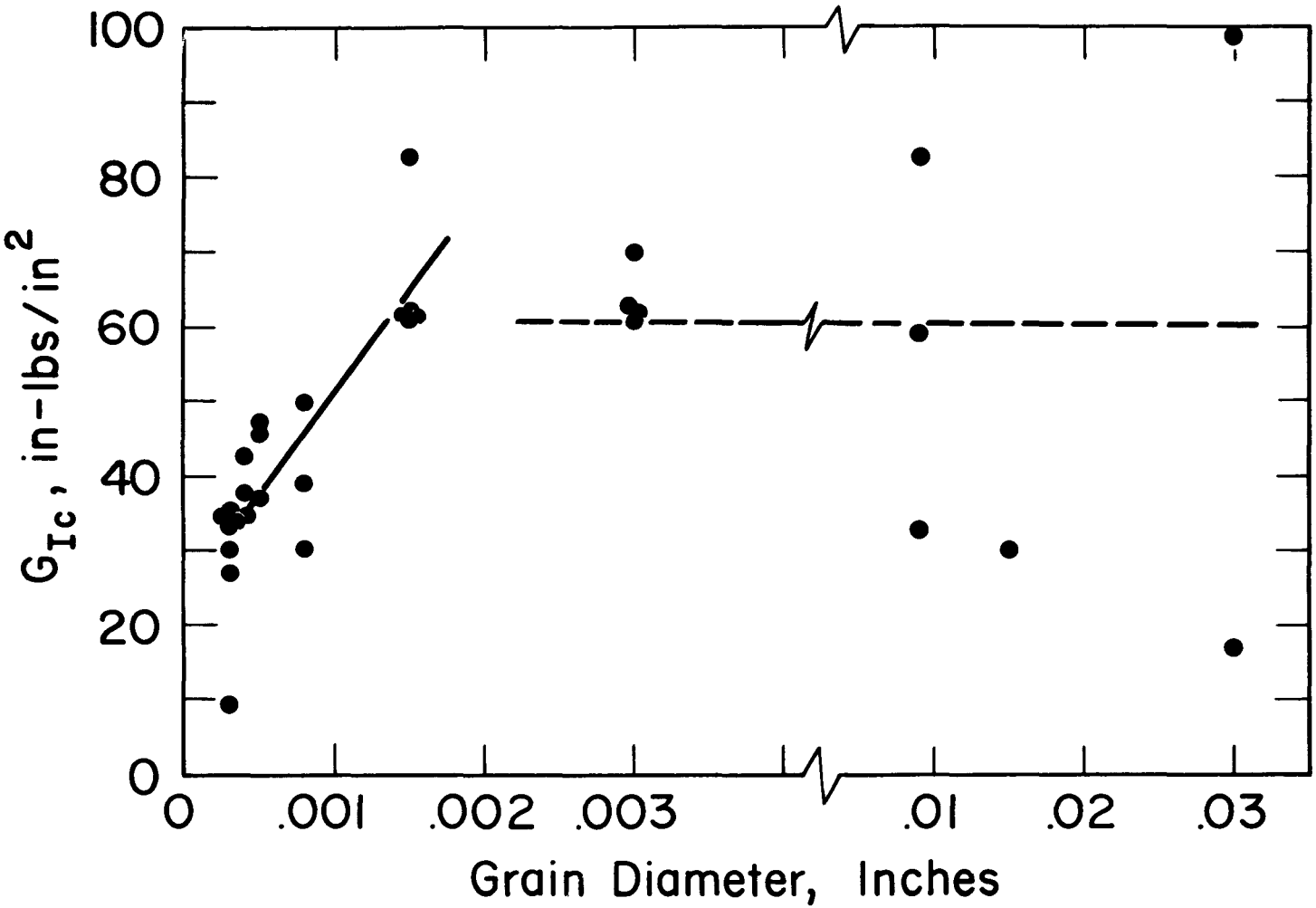

Figure C-3 - Plane strain fracture toughness, G_{IC}, as a function of prior austenite grain size.

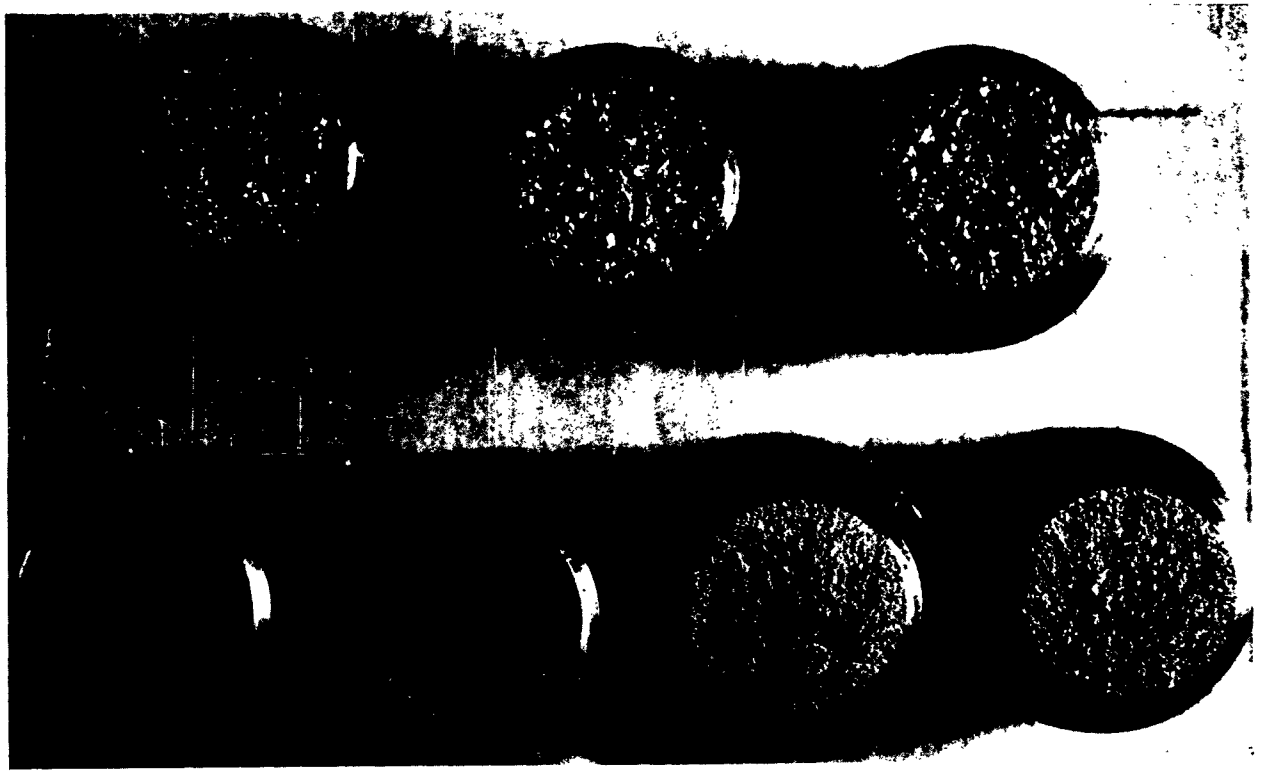

Figure C-4 - Typical fracture surfaces of notched tensile specimens. All specimens austenitized, oil quenched, refrigerated in liquid nitrogen, tempered at 400°F. Austenitizing temperatures: (bottom row, l. to r.) 1550, 1800, 2000 and 2100°F, (top row, l. to r.) 2200, 2250 and 2300°F. 2X.

among the individual samples, e.g., in specimens austenitized at 2300°F, the amount of intergranular fracture varied from something less than 50% to more than 75%.

Other evidence pointing to intergranular fracture in specimens austenitized at higher temperatures was obtained by listening with a stethoscope during loading. Clicking sounds were heard only when austenitizing had been done above about 1900°F; they were noticeable just before maximum load in specimens austenitized at 2000°F, and loads as low as 50% of the maximum in specimens austenitized at 2250 and 2300°F.

Metallographic sections of the fractured specimens also indicated increased grain-boundary separation with increasing austenitizing temperature. Typical contours are shown in Fig. C-5 and Fig. C-6. A decreased amount of banding was also evident in specimens austenitized at 2300°F (Fig. C-6b), a result of greater homogenization from such a treatment.

In many cases, narrow bands of untempered martensite were formed during fracture. These were generally observed on vertical surfaces (as in Fig. C-7) and are presumably due to adiabatic heating to local temperatures that must have exceeded about 1400°F. Such findings were made only in specimens austenitized above 2000°F.

This investigation of the effect of austenitizing temperature on plane-strain fracture toughness suggests that G_{IC} increases as the temperature of austenitizing (and the austenite grain size) is increased, until an "overheating temperature" is reached. Specimens austenitized above such a temperature exhibit extensive intergranular fracture and widely varying G_{IC} values. The tendency of AISI 4340 to fail along prior austenite grain boundaries when austenitized above about 2000°F precludes very extensive study of the relationship between G_{IC} and austenite grain size. Perhaps vacuum-melted steels may have sufficiently high overheating temperatures to permit a useful extension of the grain-size range.

The tendency of G_{IC} to increase with higher austenitizing temperatures may be related to increases either singly or in combination of a number of factors: homogenization, strain hardening, strain-rate sensitivity, grain size. A limited amount of electron microscopy has indicated that, contrary to the trend in plain-carbon steels, the martensite platelet size in AISI 4340 varied little with increasing austenite grain size. Consequently the martensite platelet size would not seem to be an important consideration.

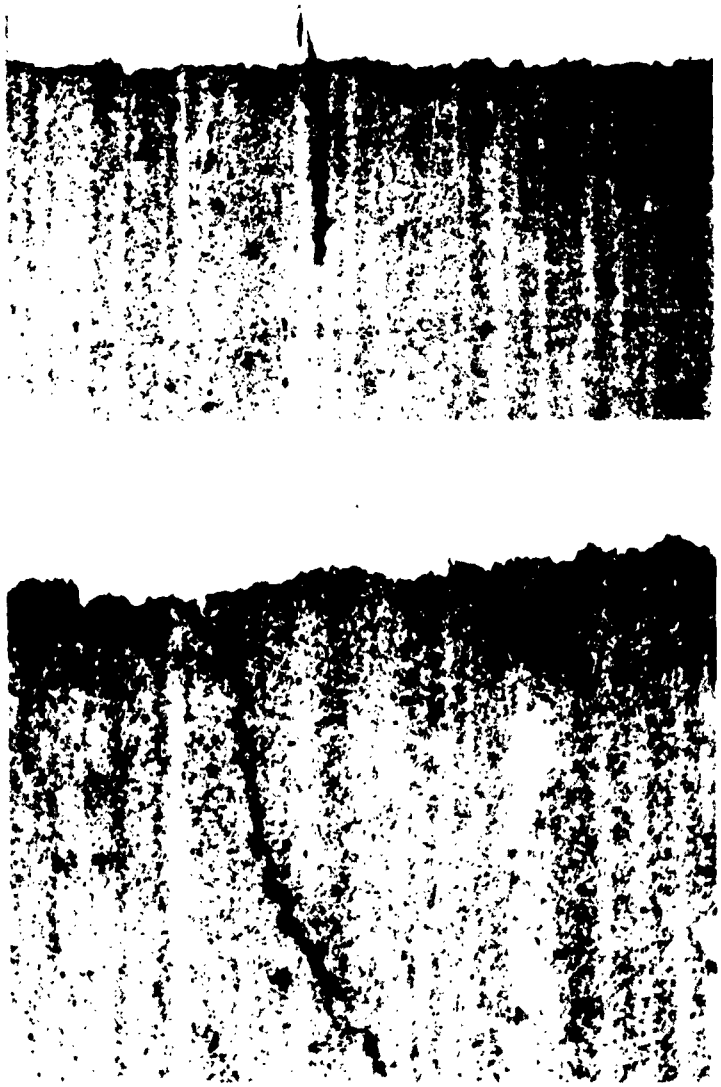

(a)

(b)

Figure C-5 - Typical longitudinal sections through fracture surfaces. Austenitizing temperatures: (a) 1550°F, (b) 1800°F. Surfaces nickel-plated prior to sectioning, 1% nital etch. 100X.

(a)

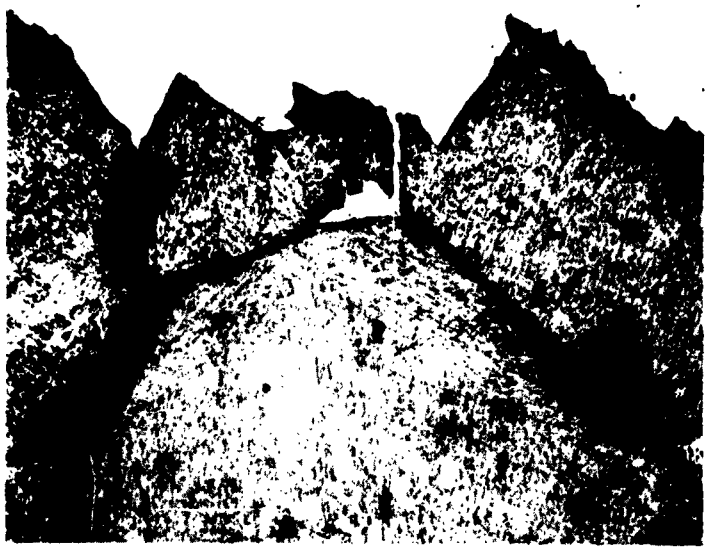

(b)

Figure C-6 - Additional longitudinal sections through fractures. Austenitizing temperatures: (a) 2000°F, (b) 2300°F. Note the clear indication of intergranular fracture and decreased banding in (b). Surfaces nickel plated prior to sectioning, 1% nital etch. 100X.

(a)

(b)

Figure C-7 - Evidence of untempered martensite formation on the fracture surface of a specimen austenitized at 2300°, oil quenched, refrigerated and tempered at 400°F. Light etching martensite shown in (a) at 2000X. Note greater hardness of white band. Photograph (b) shows same area at 100X. Note the second light-etching band on left side of the field.

DISTRIBUTION LIST

	No. of Copies
A. Department of Defense	
Office of the Director of Defense Reserch & Engineering Attn: Mr. J. C. Barrett Room 3D-1085, The Pentagon Washington 25, D. C.	1
Armed Services Technical Information Agency Attn: TIPDR Arlington Hall Station Arlington 12, Virginia	10
Defense Metals Information Center Battelle Memorial Institute Columbus, Ohio	1
Solid Propellant Information Agency Applied Physics Laboratory The Johns Hopkins University Silver Spring, Maryland	3
B. Department of the Army	
Commanding Officer Army Research Office Office Chief Research & Development Attn: Physical Sciences Division 3045 Columbia Pike Arlington, Virginia	2
Commanding General U.S. Army Materiel Command Detachment I, Room 2502, Bldg. T-7 Attn: AMCRD-RS-CM Washington 25, D. C.	1
Commanding General U.S. Army Electronics Command Attn: Mr. H. H. Kedesky Fort Monmouth, N. J.	1

DISTRIBUTION LIST (Continued)

	No. of Copies
Commanding General U.S. Army Missile Command	
Attn: Documentation & Technical Information Branch	2
Mr. R. Fink, AMSMI-RKX	1
Mr. E. J. Wheelahan, AMSMI-RSM	1
Mr. R. E. Ely	1
Mr. T. N. L. Pughe	1
Mr. E. Fohrell	1
Redstone Arsenal, Alabana	1
Commanding General U.S. Army Weapons Command Attn: Mr. B. Gerke Rock Island, Illinois	1
Commanding General U.S. Army Mobility Command U.S. Army Tank-Automotive Center Attn: Mr. S. Sobak Detroit 9, Michigan	1
Commanding General U.S. Army Munitions Command Dover, New Jersey	1
Commanding Officer Harry Diamond Laboratory Attn: Technical Library Washington 25, D. C.	4
Commanding Officer U.S. Army Chemical & Coating Laboratory Attn: Dr. C. Pickett Aberdeen Proving Ground, Maryland	1
Commanding Officer U.S. Army Materials Research Office Watertown Arsenal	
Attn: OPT	1
Technical Information Center	3
Watertown 72, Massachusetts	

	No. of Copies
Commanding Officer U.S. Army Munitions Command Frankford Arsenal Attn: Dr. H. Gisser, SMUFA-1330 Mr. H. Markus, SMUFA-1320 Mr. E. Roffman, SMUFA-1740 Philadelphia 37, Pa.	 1 1 1
Commanding Officer U.S. Army Munitions Command Picatinny Arsenal Attn: Mr. J. Matlack, Plastics & Packaging Lab. Mr. D. Stein Dover, New Jersey	 3 1
Commanding Officer U.S. Army Weapons Command Rock Island Arsenal Attn: Laboratory Rock Island, Illinois	 1
Commanding Officer U.S. Army Weapons Command Springfield Armory Attn: Research Materials Lab. Springfield 1, Mass.	 1
Commanding Officer U.S. Army Weapons Command Watervliet Arsenal Attn: Mr. F. Dashnaw Watervliet, New York	 1
Director PLASTEC Picatinny Arsenal Dover, New Jersey	 1

C. Department of the Navy

Chief, Bureau of Naval Weapons Department of the Navy Attn: RMMP Room 2225, Munitions Building Washington 25, D. C.	 1

DISTRIBUTION LIST (Continued)

	No. of Copies
Department of the Navy Office of Naval Research Attn: Code 423 Washington 25, D. C.	1
Department of the Navy Special Projects Office Attn: SP 271 Washington 25, D. C.	1
Commander U.S. Naval Ordnance Laboratory Attn: Code WM White Oak, Silver Spring, Maryland	1
Commander U.S. Naval Ordnance Test Station Attn: Technical Library Branch China Lake, California	1
Commander U.S. Naval Research Laboratory Attn: Mr. J. E. Srawley Anacostia Station Washington 25, D. C.	1
D. Department of the Air Force	
U.S. Air Force Directorate of Research & Development Attn: Lt Col J. B. Shipp, Jr. Room 4D-313, The Pentagon Washington 25, D. C.	1
Wright Air Development Division Attn: H. Zoeller, ASRCEE-1-2 R. F. Klinger, ASRCEM-1 Wright-Patterson Air Force Base, Ohio	2 2
6593 Test Group (Development) Attn: Solid Systems Division, DGSC Edwards Air Force Base, California	1
AMC Aeronautical Systems Center Attn: Manufacturing & Materials Technology Div, LMBMO Wright-Patterson Air Force Base, Ohio	2

DISTRIBUTION LIST (Continued)

	No. of Copies
E. Other Government Agencies	
U.S. Atomic Energy Commission Office of Technical Information Extension P.O. Box 62 Oak Ridge, Tennessee	1
National Aeronautics and Space Administration Attn: Mr. B. G. Achhammer Mr. G. C. Deutsch Mr. R. V. Rhode Washington, D. C.	1 1 1
Geroge C. Marshall Space Flight Center Attn: Dr. W. Lucas, M-S&M-M Mr. W. A. Wilson, M-ME-M Huntsville, Alabama	1 1
Dr. L. Jaffe Jet Propulsion Laboratory California Institute of Technology 4800 Oak Grove Drive Pasadena, California	1
F. Defense Contractors	
Aerojet-General Corporation Attn: Librarian Post Office Box 1168 Sacramento, California	1
Aerojet-General Corporation Attn: Mr. C. A. Fournier Post Office Box 1947 Sacramento, California	1
Aerojet-General Corporation Attn: Librarian Azusa, California	1
Allison Division General Motors Corporation Attn: Mr. D. K. Hanink Indianapolis 6, Indiana	1

DISTRIBUTION LIST (Continued)

	No. of Copies
ARDE-Portland, Inc. Attn: Mr. R. Alper 100 Century Road Paramus, N. J.	1
Atlantic Research Corporation Attn: Mr. E. A. Olcott Shirley Highway and Edsall Road Alexandria, Virginia	1
Boeing Company Aerospace Division Attn: Mr. R. R. Barber, Library Unit Chief Post Office Box 3707 Seattle 24, Washington	1
Curtiss-Wright Corporation Wright Aeronautical Division Attn: Mr. A. M. Kettle, Technical Library Wood-Ridge, N. J.	1
Hercules Powder Company Allegheny Ballistics Laboratory Attn: Dr. R. Steinberger Post Office Box 210 Cumberland, Maryland	1
Hughes Aircraft Company Attn: Librarian Culver City, California	1
Narmco Research & Development Attn: Technical Library 3450 Aero Court San Diego 23, California	1
Rohm & Haas Company Redstone Arsenal Division Attn: Library Redstone Arsenal, Alabana	1

DISTRIBUTION LIST (Continued)

	No. of Copies
Tapco Group Attn: Mr. W. J. Piper 23555 Euclid Avenue Cleveland 17, Ohio	1
Thickol Chemical Corp. Redstone Division Attn: Library Redstone Arsenal, Alabama	1

SUPPLEMENTAL DISTRIBUTION LIST

	No. of Copies
A. Department of the Navy	
Chief, Bureau of Naval Weapons Department of the Navy Attn: Mr. P. Goodwin Mr. H. Boertzel Washington 25, D. C.	1 6
Commander U.S. Naval Research Lab. Attn: Mr. E. Kohn, Code 6110 Washington 25, D. C.	1
B. Department of the Air Force	
Headquarters Aeronautical Systems Division Attn: Dr. Tamborski, ASRCNP Wright-Patterson Air Force Base, Ohio	1
Wright Air Development Division Attn: Mr. G. Peterson, ASRCNC-1 Wright-Patterson Air Force Base, Ohio	1
C. Defense Contractors	
Allegheny Ludlum Steel Corporation Research Center Attn: Mr. R. A. Lula Brackenridge, Pennsylvania	1
Alloyd Electronics Corporation Attn: Dr. S. S. White 35 Cambridge Parkway Cambridge, Mass.	1
Aluminum Company of America Alcoa Research Labs. Attn: Dr. J. L. Brandt Post Office Box 772 New Kensington, Pa.	1
Armco Steel Corporation General Offices Attn: Mr. J. Barnett Middletown, Ohio	1

SUPPLEMENTAL DISTRIBUTION LIST (Continued)

	No. of Copies
Battelle Memorial Institute Attn: Mr. R. Monroe 505 King Avenue Columbus 1, Ohio	1
Borg-Warner Corporation Ingersoll Kalamazoo Division Attn: Mr. L. E. Hershey 1810 N. Pitcher St. Kalamazoo, Michigan	1
The Budd Company Defense Division Attn: Mr. R. C. Dethloff Philadelphia 32, Pennsylvania	1
Climax Molybdenum Company Attn: Mr. R. R. Freeman 1270 Avenue of the Americas New York 20, N. Y.	1
Crucible Steel Co. of America Attn: Mr. W. L. Finlay Four Gateway Center Pittsburgh 22, Pa.	1
Douglas Aircraft Company Inc. Santa Monica Division Attn: Mr. J. L. Waisman Santa Monica, California	1
E. I. Du Pong Nemours and Co. Eastern Laboratories Attn: Mr. C. P. Williams Mr. J. J. Douglass Wilmington 98, Delaware	1 1
General Electric Company Rocket Engine Section Flight Propulsion Laboratory Department Cincinnati 15, Ohio	1
H. I. Thompson Fiber Glass Co. 1600 West 135th Street Gardena, California	1

SUPPLEMENTAL DISTRIBUTION LIST (Continued)

	No. of Copies
Kaiser Aluminum & Chemical Corp. Spokane Washington	1
A. D. Little, Inc. Attn: Dr. R. Davis Acorn Park Cambridge 40, Mass.	1
Ladish Company Attn: Mr. R. P. Daykin Cudahy, Wisconsin	1
Lyon, Inc. Attn: Mr. W. Martin 13881 W. Chicago Boulevard Detroit, Michigan	1
Manufacturing Laboratories Attn: Dr. V. Radcliffe 21-35 Erie Street Cambridge 42, Mass.	1
Minneapolis-Honeywell Regulator Co. 1230 Soldier Field Road Brighton 35, Mass.	1
Norris-Thermador Corporation Attn: Mr. L. Shiller 5215 South Boyle Avenue Los Angeles 58, California	1
The Perkin-Elmer Corporation Attn: Mr. H. L. Sachs Main Avenue Norwalk, Connecticut	1
Pratt & Whitney Aircraft Attn: Mr. F. A. Corsby East Hartford, Connecticut	1
Reactive Metals Corporation Attn: Mr. H. Lundstrem Niles, Ohio	1

SUPPLEMENTAL DISTRIBUTION LIST (Continued)

	No. of Copies
Republic Aviation Company Missile Systems Division Attn: R. Stegler 223 Jericho Turnpike Mineola, N. Y.	1
Republic Steel Corporation Research Center Attn: Mr. H. P. Manger 6801 Brecksville Road Cleveland 31, Ohio	1
Space Technology Laboratories, Inc. Attn: Technical Information Center Document Procurement Post Office Box 95001 Los Angeles 45, California	1
Thickol Chemical Corporation Utah Division Brigham City, Utah	1
Thickol Chemical Corporation Reaction Motors Division Denville, New Jersey	1
Thompson Ramo Wooldridge, Inc. Tapco Group Attn: W. J. Piper 207 Hindry Avenue Inglewood, California	1
Titanium Metals Corporation Attn: Mr. G. Erbin 233 Broadway New York, N. Y.	1
Universal-Cyclops Steel Corp. Stewart Street Bridgeville, Pennsylvania	1
U.S. Borax Research Corp. Attn: Mr. R. J. Brotherton 412 Crescent Way Anaheim, California	1

SUPPLEMENTAL DISTRIBUTION LIST (Continued)

	No. of Copies
United States Rubber Company Research Center Attn: Dr. E. J. Joss Wayne, N. J.	1
Wyman-Gordon Company Attn: Mr. A. Rustay Grafton, Mass.	1
D. Educational Institutions	
Massachusetts Institute of Technology Attn: Prof. W. A. Backofen Prof. M. C. Flemings Cambridge, Massachusetts	1 1
Mellon Institute Attn: Dr. H. L. Anthony Mr. C. J. Owen 4400 Fifth Avenue Pittsburgh 13, Pa.	1 1
Michigan State University Attn: Mr. R. N. Hammer Department of Chemistry East Lansing, Michigan	1
Ohio State University Research Foundation Attn: Dr. R. McMaster Columbus, Ohio	1

AD_____ Accession No._____
Massachusetts Institute of Technology, Cambridge, Mass.
METALLURGICAL ASPECTS OF FRACTURE AT HIGH STRENGTH LEVEL
W. A. Backofen and M. L. Ebner

Report No. WAL TR 310.24/5-4, May 1963
25 pp - Tables - Illustrations
OMS Code 5010.11.843, Unclassified Report

The plane-strain fracture toughness of quenched and tempered AISI 4340 steel was measured in tension at *room temperature with circumferentially notched and* fatigue-cracked specimens. Values of G_{IC} for indicating the variation encountered were 5.6, 23, and 254 in-lbs/in^2 *after tempering at* 212, 400, and 800°F, respectively.

Cracking characteristics were influenced by tempering temperature. Below about 700°F, little stable crack growth was found and propagation occurred in a mixed *mode that appeared to consist at least partly of* cleavage fracture. At higher temperatures, initial cracking was stable and developed by a ductile shear *process; rapid fracturing again occurred in a mixed* mode. After tempering at 1000°F and above, fracture was ductile.

NO DISTRIBUTION LIMITATIONS

UNCLASSIFIED

1. Steel, Physical and Mechanical Properties
2. Fracture Toughness
3. Rocket Motor Cases

I. W. A. Backofen and M. L. Ebner, Massachusetts Institute of Technology

II. OMS Code 5010.11.843

AD_____ Accession No._____
Massachusetts Institute of Technology, Cambridge, Mass.
METALLURGICAL ASPECTS OF FRACTURE AT HIGH STRENGTH LEVEL
W. A. Backofen and M. L. Ebner

Report No. WAL TR 310.24/5-4, May 1963
25 pp - Tables - Illustrations
OMS Code 5010.11.843, Unclassified Report

The plane-strain fracture toughness of quenched and tempered AISI 4340 steel was measured in tension at room temperature with circumferentially notched and fatigue-cracked specimens. Values of G_{IC} for indicating the variation encountered were 5.6, 23, and 254 in-lbs/in^2 after tempering at 212, 400, and 800°F, respectively.

Crackirg characteristics were influenced by temperirg temperature. Below about 700°F, little stable crack growth was found and propagation occurred in a mixed mode that appeared to consist at least partly of cleavage fracture. At higher temperatures, initial crackirg was stable and developed by a ductile shear process; rapid fracturing again occurred in a mixed mode. After tempering at 1000°F and above, fracture was ductile.

NO DISTRIBUTION LIMITATIONS

UNCLASSIFIED

1. Steel, Physical and Mechanical Properties
2. Fracture Toughness
3. Rocket Motor Cases

I. W. A. Backofen and M. L. Ebner, Massachusetts Institute of Technology

II. OMS Code 5010.11.843

AD_____ Accession No._____
Massachusetts Institute of Technology, Cambridge, Mass.
METALLURGICAL ASPECTS OF FRACTURE AT HIGH STRENGTH LEVEL
W. A. Backofen and M. L. Ebner

Report No. WAL TR 310.24/5-4, May 1963
25 pp - Tables - Illustrations
OMS Code 5010.11.843, Unclassified Report

The plane-strain fracture toughness of quenched and tempered AISI 4340 steel was measured in tension at room temperature with circumferentially notched and fatigue-cracked specimens. Values of G_{IC} for indicating the variation encountered were 5.6, 23, and 254 in-lbs/in^2 after tempering at 212, 400, and 800°F, respectively.

Cracking characteristics were influenced by tempering temperature. Below about 700°F, little stable crack growth was found and propagation occurred in a mixed mode that appeared to consist at least partly of cleavage fracture. At higher temperatures, initial cracking was stable and developed by a ductile shear process; rapid fracturing again occurred in a mixed mode. After tempering at 1000°F and above, fracture was ductile.

NO DISTRIBUTION LIMITATIONS

UNCLASSIFIED

1. Steel, Physical and Mechanical Properties
2. Fracture Toughness
3. Rocket Motor Cases

I. W. A. Backofen and M. L. Ebner, Massachusetts Institute of Technology

II. OMS Code 5010.11.843

AD_____ Accession No._____
Massachusetts Institute of Technology, Cambridge, Mass.
METALLURGICAL ASPECTS OF FRACTURE AT HIGH STRENGTH LEVEL
W. A. Backofen and M. L. Ebner

Report No. WAL TR 310.24/5-4, May 1963
25 pp - Tables - Illustrations
OMS Code 5010.11.843, Unclassified Report

The plane-strain fracture toughness of quenched and tempered AISI 4340 steel was measured in tension at *room temperature with circumferentially notched and* fatigue-cracked specimens. Values of G_{IC} for indicating the variation encountered were 5.6, 23, and 254 in-lbs/in^2 *after tempering at* 212, 400, and 800°F, respectively.

Cracking characteristics were influenced by tempering temperature. Below about 700°F, little stable crack growth was found and propagation occurred in a mixed *mode that appeared to consist at least partly of* cleavage fracture. At higher temperatures, initial cracking was stable and developed by a ductile shear *process; rapid fracturing again occurred in a mixed* mode. After tempering at 1000°F and above, fracture was ductile.

NO DISTRIBUTION LIMITATIONS

UNCLASSIFIED

1. Steel, Physical and Mechanical Properties
2. Fracture Toughness
3. Rocket Motor Cases

I. W. A. Backofen and M. L. Ebner, Massachusetts Institute of Technology

II. OMS Code 5010.11.843